Structural proteomics defines a sequential priming mechanism for the progesterone receptor

Matthew D. Mann[1,2], Min Wang[3], Josephine C. Ferreon[5], Michael P. Suess[3], Antrix Jain[4], Anna Malovannaya[5], Bruce D. Pascal[6], Raj Kumar[7], Dean P. Edwards[3], and Patrick R. Griffin[*,1,2]

[1]Skaggs Graduate School of Chemical and Biological Sciences, The Scripps Research Institute, Jupiter, FL, USA.

[2]Department of Molecular Medicine, The Herbert Wertheim UF Scripps Institute for Biomedical Innovation & Technology, Jupiter, FL, 33458

[3] Department of Molecular and Cellular Biology, Baylor College of Medicine, Houston, TX, 77030 USA.

[4] Mass Spectrometry Proteomics Core Facility. Advanced Technology Cores, Baylor College of Medicine, Houstonm TX, 77030

[5] Verna and Marrs McLean Department of Biochemistry and Molecular Pharmacology, Baylor College of Medicine, Houston, TX, 77030

[6] Omics Informatics LLC. 1050 Bishop Street #517, Honolulu, HI 96813

[7] Department of Pharmaceutical and Biomedical Sciences, Touro College of Pharmacy, Touro University, New York, NY, USA.

* Correspondence should be addressed to pgriffin2@ufl.edu

Running title: Structural proteomics reveals a unique activation model for PR-A and PR-B

Acknowledgements: This work was supported by NIH-NCI R01 (CA263574) to MPIs, PRG, RK, and DPE. The authors acknowledge the expert assistance of the Recombinant Protein Production and Characterization Core (RPPCC) for expression of recombinant proteins in the baculovirus insect cell system and the Mass Spectrometry Proteomcs (MSPC) Core for amino acid sequencing and phosphorylation analysis of recombinant proteins. The RPPCC and MSPC at BCM are supported by the NCI Cancer Center Support Grant (P30 CA125123) of the Dan L Duncan Comprehensive Cancer Center and the MSPC is additionally supported by a CPRIT (Cancer Prevention and Research Institute of Texas) Core Facility Support Award (RP210227). Additional support is from NIH S10 Shared Instrument Grant (1S10OD030276) to JCF for the SEC-MALS instruments.

Keywords:

Progesterone receptor; hydrogen-deuterium exchange; crosslinking; mass spectrometry; protein-protein interactions; nuclear receptors, transcriptional co-regulatory proteins

Abstract

The progesterone receptor (PR) is a steroid-responsive nuclear receptor, expressed as two isoforms: PR-A and PR-B. The isoforms display distinct expression patterns and biological actions in reproductive target tissues and disruption of PR-A:PR-B signaling is associated with breast cancer development potentially by altering interactions with oncogenic co-regulatory protein (CoRs). However, the molecular details of isoform-specific PR-CoR interactions that influence progesterone signaling remain poorly understood. We employed structural mass spectrometry in this study to investigate the sequential binding mechanism of purified full-length PR and full-length CoRs, steroid receptor coactivator 3 (SRC3) and p300, as complexes with target DNA. Our findings reveal selective CoR NR-box binding by PR and novel interaction surfaces between PR, SRC3, and p300, which change during complex assembly. This provides a structural model for a sequential priming mechanism that activates PR. Comparisons of PR bound to progesterone agonist versus antagonist challenges the classical model of nuclear receptor activation and repression. Collectively, we offer a peptide-level perspective on the organization of the PR transcriptional complex and elucidate the mechanisms behind the interactions of these proteins, both in active and inactive conformations.

Introduction

The progesterone receptor (PR) is a steroid-activated nuclear receptor and belongs to the subfamily of steroid hormone receptors (SRs) that includes the estrogen receptor, androgen receptor, mineralocorticoid receptor, and glucocorticoid receptor. The SRs, including PR, exhibit remarkable functional diversity in mediating cell/tissue and target gene-specific responses, largely driven by conformational dynamics of the protein that enables its binding to DNA response elements and unique subsets of co-regulatory proteins (CoRs). Like other SRs, PR is a modular protein composed of well-folded ligand binding (LBD) and DNA binding (DBD) domains that are connected via a structurally dynamic hinge region, and an intrinsically disordered (ID) N-terminal domain (NTD). The hinge, additionally termed carboxyl terminal extension (CTE), is more than a flexible linker. It forms an extended loop that interacts with the minor groove of DNA flanking either side of inverted repeat progesterone response element (PREs) to extend the protein-DNA interface beyond that of the core DBD that binds major groove of HREs.[1, 2] SRs also contain two transcriptional activation functions, ligand-independent AF1 in the NTD and ligand-dependent AF2 in the LBD, that provide interaction surfaces for CoRs.[3-5]

PR is important for development, proliferation and differentiation of female reproductive tissues during the reproductive cycle and pregnancy.[6-11] The biological response to progesterone is mediated by two distinct protein isoforms: PR-A and PR-B, that are expressed through alternate utilization of two promoters of the same gene. PR-A is an N-terminal truncation (missing aa 1-165) of full-length PR-B, with each having distinct cell/tissue-dependent physiological roles. Generally, PR-A is a weaker transcriptional activator than PR-B, and both isoforms are typically co-expressed in equal proportions in most normal tissues. However, their ratios have been reported to be highly variable in pathological conditions. Both PR isoforms contribute to the onset of breast cancer, and increased expression of PR-A has been shown to alter progestin responsiveness in cancer phenotypes. Interestingly, known CoRs are shared between isoforms, yet each isoform's transcriptional activity differs. The mechanistic basis for differences in the activity of the isoforms remains unclear but is generally believed to be due to differences yet to be determined in structural conformations and, thereby, CoR interactions.[10, 12-14]

To more fully understand PR's biology requires detailed structural analysis of the full-length PR isoforms, associated with full-length CoRs as a complex on target DNA, and an understanding of how protein interactions within the complex and structural conformations can affect the activity of PR. The conformational flexibility of SRs and CoRs, coupled with their large sizes, make them unsuitable for either high-resolution NMR or X-ray crystallography analysis. Recent low-resolution cryoEM studies using PR:SRC2:p300 complex also failed to provide details of specific interactions of PR with CoRs at the atomic level, thus limiting the utility of these analyses. [4, 10, 12, 15-26] Here, we present an amino-acid resolution view of canonical PR-A and PR-B transcriptional complex, including SRC3 and p300, on PR target DNA. High resolution crystal structures have been determined for the PR DBD-CTE[1] complexed with a consensus inverted repeat palindromic progesterone response element (PRE) DNA, and the PR LBD complexed with a progesterone agonist[27] or antagonists with a peptide from a

transcriptional co-repressor.[28, 29] However, there is a lack of structural detail for full-length PR and CoRs as a complex with PRE DNA.[28, 30-32]

An alternative to classical structural techniques is structural proteomics. Hydrogen-deuterium exchange (HDX) works on the principle of backbone amide exchange, where protein backbone amide hydrogens will freely exchange to deuterium upon regular protein motion.[33-37] This is a useful technique for measuring differences in deuterium exchange, which informs protein conformational changes and protein-protein interaction sites. Similarly, crosslinking (XL) coupled with mass spectrometry provides information on amino acid proximity.[38-41] Chemical crosslinkers provide information on protein proximity, which is useful in determining protein-protein interaction regions. By using a combination of HDX-MS and XL-MS, we gain a higher-resolution functional understanding of the organization of these complexes compared to the available electron microscopy structures. These data show that PR interacts with SRC3 and p300 in an isoform-specific and ligand-specific manner that may impart the distinct function of each. The structural information gained from our studies is essential for advancing our understanding of the molecular mechanism of action of PRs and other SRs.

Results

Strep-II tagged Recombinant PR and CoRs generates stable protein and complexes:

Intact full-length PR and CoRs were expressed and purified as recombinant proteins in Sf9 insect cells using the baculovirus system.[42] This is an ideal expression system for full-length PR shown previously to retain native folding and post-translational modifications including phosphorylation on the same sites as occurs with endogenous PR in mammalian cell types.[43, 44] Additionally purified full-length PR from the baculovirus system was demonstrated to exhibit stoichiometric ligand binding activity, high affinity binding to specific progesterone response element (PRE) DNA, including free DNA and when assembled on nucleosomes, and transcriptional activity in cell-free assays.[42, 45-48] As a refinement of our previous methods for expression and purification of PR, a Strep-II affinity tag at the N-terminus of PR was used in place of poly-histidine.[44, 49] Strep II is a minimal eight amino-acid peptide that binds to the core of streptavidin and due to its high-affinity and low non-specific interactions has superior properties for efficient affinity purification of recombinant fusion proteins using immobilized variants of streptavidin. Since the Strep-II tag is biologically inert and does not affect protein folding, it is potentially ideal for isolation of large multi-domain proteins such as PR and CoR in their intact native state.[50] Strep II tagged PR-A or PR-B were expressed in Sf9 insect cells in the presence of the progestin ligand agonist R5020 to activate the receptor in culture. As described in more detail in Methods, receptors in native cell lysates were bound to a StrepTrap XT (Cytiva) affinity resin on an AKTApure 25 FPLC system and after extension washing bound protein was eluted with biotin and submitted to a second step purification by Superdex S200 size exclusion chromatography (SEC). The SEC fractions from the major protein peak that correspond with the expected molecular size of monomeric PR were pooled and concentrated in the range of 1.5mg-1.6mg/ml (15uM-

18uM) with yields between 2.25 to 2.4mg of total protein from 1 liter of Sf9 cells. As assessed by SDS-PAGE, each PR isoform contained a single major protein band of expected molecule size with a purity > 98% (**Supplementary Figure 1 [Figure S1]**). Yields were higher than with poly-histidine tagged PR from previous work, presumably due to the greater efficiency of Strep II tagged affinity system that results in fewer contaminating proteins and more enriched PR as a single purification step. Mass spectrometry sequencing with a coverage > 89% confirmed the identity of major protein bands of purified PR-A and PR-B as intact full-length PR-A or PR-B with no other peptides identified from unrelated insect cell protein background (**Fig S2**). However, purified PR-B typically contained a faint band (~2% of total) running slightly smaller than the major band, suggestive of a degradation fragment of PR. However, further mass spectrometry analysis of the smaller sized band showed it is also intact full-length PR-B with a slightly different phosphorylation pattern (**Fig S3**) than the major band. Phosphorylation of PR is known to alter its mobility on SDS-PAGE.[43] The nuclear co-regulatory proteins SRC3 and p300 as full-length constructs with Strep II tags at the amino terminus were expressed in Sf9 insect cells and purified in a similar two-step procedure with the StrepTrap XT affinity column, elution with biotin and size exclusion chromatography by Superdex 200. This resulted in SRC3 (**Figure S4)** and p300 **(Figure S5**) each exhibiting a single major band on SDS-PAGE of expected molecular size at >98% purity. The concentrations of purified SRC3 and p300 were in the range of 2.0-2.5mg/ml (12uM and 9uM) with yields of 2.0-2.5 total mg from 1 liter of insect cell cultures. Mass spectrometry confirmed the identity of SRC3 and p300 each as intact full-length protein with no detectable other unrelated insect cell peptides (**Figure S6**).

Quality of purified proteins and DNA-induced dimerization of PR.

The quality of purified proteins was further assessed by size-exclusion chromatography-multi-angle light scattering (SEC-MALS) and differential scanning fluorimetry (DSF). We performed SEC-MALS for each purified individual protein and DNA, as well as various mixtures of the different proteins and DNA. SEC-MALS chromatograms for each individual protein displayed single peaks with experimentally derived molecular weights (MW) within the expected theoretical MW for each macromolecule as a monomer except PR-B that behaved as a mixture of monomer and dimer **(Figure 1 and Table S1).** Slight discrepancies between experimental and theoretical MW of individual proteins (e.g., PR-A, SRC3, p300) observed were likely due to deviation of dn/dc values from that of BSA. BSA is a globular protein while PR-A, SRC3 and p300 have significant disordered regions. In the absence of DNA, PR-A bound to the progestin agonist ligand R5020 showed monomeric molecular weight distribution and with addition of DNA assembled as a complex with an experimentally determined MW within the expected theoretical for a PR-A dimer (**Figure 1 and Table S1)**. PR-B liganded with R5020 gave a mixture of monomer and dimer MW distributions in the absence of DNA and a single MW distribution within the expected theoretical for a PR-B dimer upon assembly as a complex with DNA **(Figure 1 and Table S1).** These results are consistent with previous data showing that PR binds to PRE DNA as a dimer and further indicates that DNA induces formation of stable dimers. SEC-MALS also detected a higher order complex assembly of all three proteins (PR-A R5020 agonist-bound, SRC3, p300) with DNA that eluted slightly ahead of that of p300 analyzed alone as observed in the SEC-MALS chromatogram **(Figure S7, top panel**).

The peak of the protein mixture had a long tail and showed heterogeneous MW distribution, indicating some overlap with single protein monomeric p300 and SRC3. Experimentally determined MW analysis indicated formation of a 540 kDa complex for the peak apex, which could reflect weighted averages of a 1:1:2:1 p300:SRC3:PR-A:DNA complex (expected MW~612 kDa) and monomeric p300 (expected MW=267 kDa). We could also observe the presence of DNA in the peak apex (**Figure S7**), and the consequent disappearance of a distinct peak for single SRC3 when all three proteins were added confirming the formation of the higher order complex. These data are consistent with a stoichiometry of 1 p300: 1 SRC3: 2 PR: 1 DNA in the complex in agreement with course PR:SRC2:p300/DNA CryoEM structure previously reported.[51]

DSF was used to determine the native folded state of each purified protein and stability to thermal denaturation. Proteins were incubated with SYPRO Orange, a dye that interacts with hydrophobic regions that become exposed during denaturation and can be used as a readout of protein unfolding Thermal denaturation was conducted using a LightCycler 480 thermal cycler with controlled heating from 10 °C to 95 °C at a constant rate of 0.5 °C/s and fluorescence emission was measured at various time points. For all proteins analyzed (PR-A, PR-B, SRC3 and p300) thermal denaturation emission curves were indicative of cooperative unfolding transitions with melting temperatures (T_M) in the range of 40C to 49C, indicative of moderately stable structured proteins **(Figure S8, Table S2).** Addition of PRE DNA increased the T_M of PR-A and PR-B consistent with increased stability of PR dimers as a complex with DNA **(Table S2).**

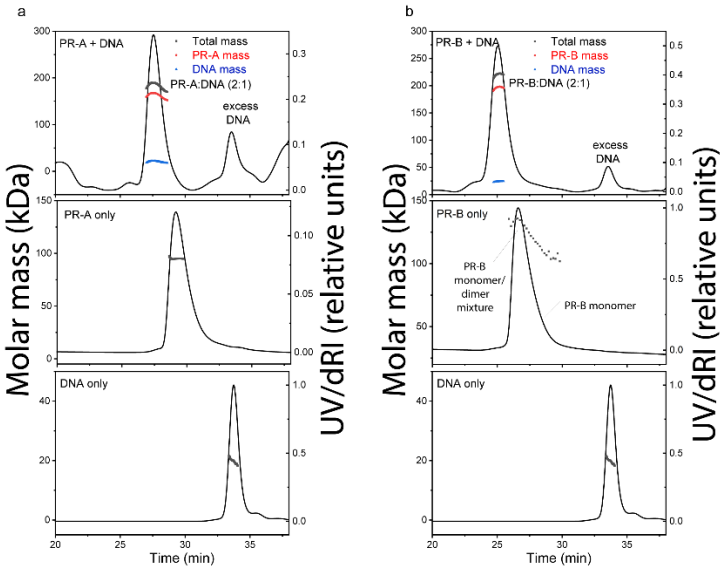

Figure 1. DNA induces assembly of PR-A and PR-B. ***A-B.*** *SEC-MALS chromatograms of agonist (R5020)- bound PR-A (A) and PR-B (B) with and without DNA. The molar mass of DNA and PR-A alone matches the monomeric molar mass (black line/dots across the peaks). DNA induces assembly of both PR-A and PR-B into a complex with 2:1 (protein:DNA) stoichiometry. The presence of DNA in the complexes were confirmed by deconvolution of the protein and DNA fractions in the peak (red and blue lines, respectively).*

DNA binding induces PR isoform specific conformational changes

Continuous labeling differential hydrogen-deuterium exchange[35] mass spectrometry (HDX-MS) has been used previously to assess hydrogen exchange on PR with transcription factor TBP[46, 47]; however, these samples were limited by overall protein coverage. Different proteases were used to probe conformational changes in full-length PR-A and PR-B upon DNA and CoR binding. The overall coverage was greatly increased across PR and CoRs with their results indicating that both the conformational changes across PR domains and the magnitude of perturbation in deuterium exchange induced by DNA binding differ between the PR-A/PRE and PR-B/PRE complexes (**Figure 2**). A comparison of the intrinsic deuterium exchange of non-DNA-bound PR-A and PR-B shows that the profiles are similar between the two isoforms (**Figure S9**), indicating that the observed

changes in solvent exchange are due to the addition of a binding partner. As shown in **Figure 2**, the addition of PRE DNA resulted in decreased deuterium exchange throughout the PR-A DBD and LBD, indicating stabilization of these domains mediated by DNA binding and suggesting DBD-LBD communication induced by DNA. Differential HDX of PR-B revealed that overall, there were less perturbations within regions of the NTD, DBD-CTE, and LBD in response to PRE binding when compared to PR-A. Although the magnitude of deuterium exchange is less than that observed with PR-A, these results indicate increased stability throughout the PR-B dimer. For example, decreased solvent exchange observed within the LBD region of PR-B, which corresponds to helix 10/11 (**Figure 2**), is part of the dimerization domain within the PR homodimer.[27] PRE-induced dimerization of the receptor was shown using SEC-MALS, showing that when PRE is present, PR-A and PR-B exhibit molecular weights within 5% of their homodimer masses when in complex with PRE at a 2:1 (PR:DNA) ratio (**Table S1**). Thus, alterations in deuterium exchange are likely a combination of homodimerization and DNA binding. Interestingly, decreased solvent exchange was observed in the PR-B NTD (amino acids 270-276), which is not observed in PR-A, potentially indicative of a shift in NTD-LBD intraprotein interactions that only exist for PR-B.

Crosslinking mass spectrometry (XL-MS) was used to assess amino acid residue and domain-domain proximity, which can inform inter and intradomain interactions. Crosslinks unique to the unbound or PRE-bound state of PR indicate that there is rearrangement between the CTE (C-terminal extension) and the LBD only when PRE is present, which suggests compaction of those regions upon DNA binding (**Figure 2**). Concurrently, crosslinks from the N-terminus to C-terminus (amino acids 240-933) are diminished, indicating that these PR domains are no longer in proximity. This may be the result of PR stabilization through homodimerization. Similar to that observed with PR-A, XL-MS results with PR-B show crosslinks from the N-terminus to C-terminus (amino acid 7 to 933) are enriched in the absence of DNA. The reduction of these N- to C-term crosslinks upon DNA binding indicates that these regions are no longer in proximity, although other crosslinks that are not near C-terminus are retained. This suggests a movement of the PR NTD away from the end of the protein, potentially showing that in the absence of DNA, the PR NTD is stabilized through NTD-LBD interactions. When bound to a canonical PRE, changes in crosslinks indicate PR rearranges to shift the NTD slightly away from the LBD, and these interactions are no longer required for protein stability (**Figure 2**).

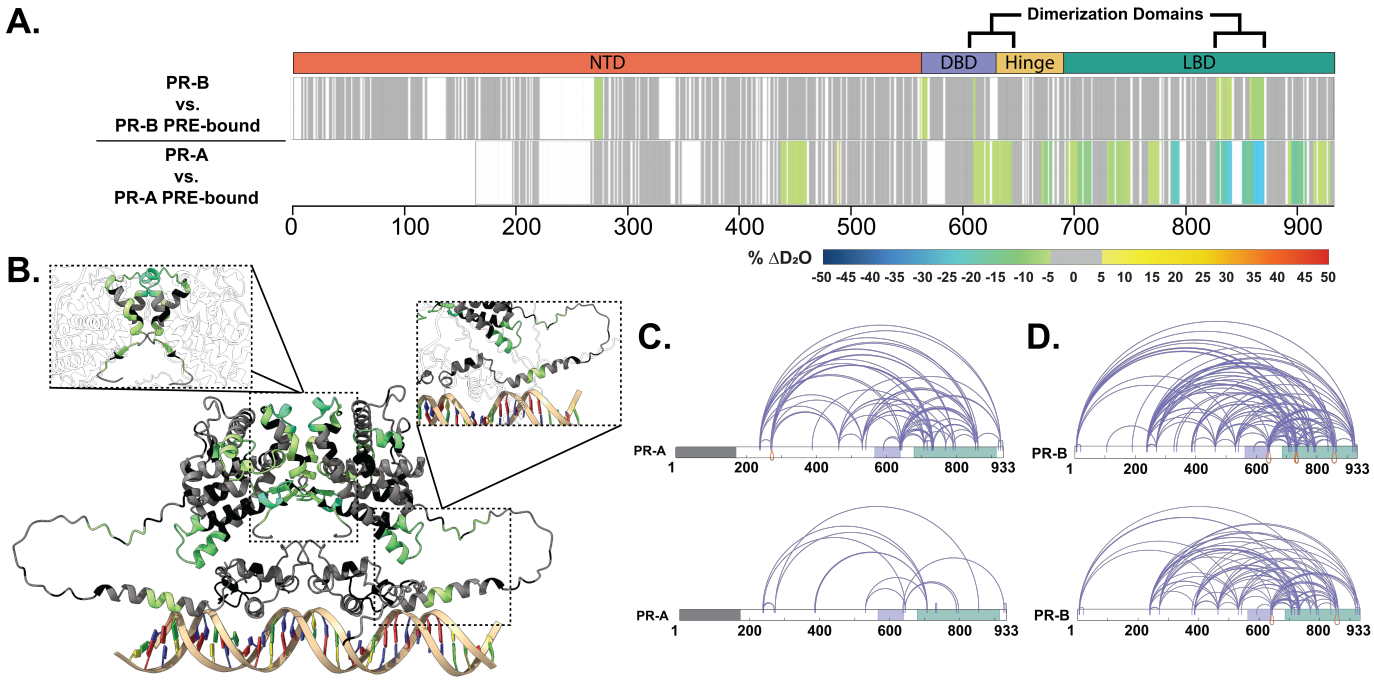

Figure 2. Structural proteomics reveals isoform differences upon response element binding. ***A.*** *Consolidated HDX-MS data, run in triplicate, showing the differential analysis between unbound PR vs. PRE-bound where the top is PR-B, and the bottom is PR-A. Domains are labeled as the following: N-terminal Domain (NTD), DNA-binding domain (DBD), Hinge region (Hinge), and Ligand binding domain (LBD).* ***B.*** *Trimmed AlphaFold 3.0 model (residues 375-769) of PR-A homodimer with unbound PR-A vs. PR-A:PRE HDX overlays. Highlighted regions are the PR dimerization domain (top) and the DBD C-terminal extension (bottom). Cooler colors indicate stronger HDX protection.* ***C.*** *XlinkX images of differential PR-A ± PRE experiments, where crosslinks from the unbound (top) and PRE-bound (bottom) states are shown. Crosslinks mapped onto PR-B numbering with the gray region representing the 164 amino acids not expressed in PR-A. Results representative of triplicate experiments, with validation in Skyline.* ***D.*** *XlinkX view of differential PR-B ± PRE experiments, where crosslinks from unbound (top) and PRE-bound (bottom) states are shown. Domains – Gray: Not expressed; Purple: DBD; Green: LBD.*

Co-regulator binding induces conformational changes to each PR isoform

Next, deuterium exchange was assessed for SRC3-bound complexes, compared to the PR homodimer alone. Using a sequential CoR addition strategy, the differential deuterium uptake of PR was measured against the PR:SRC3 complex at the stoichiometries discerned from the SEC-MALS data (2:1:1; PR:SRC3:PRE; **Figure S7**). Reduced deuterium exchange was observed throughout PR-A (**Figure 3**). This suggests that SRC3 can bind PR-A in a monomeric state in the absence of DNA. SRC3-mediated exchange protection was not centralized around a specific PR-A domain. Some interesting regions were the dimerization domains and the N-terminal domain which have reduced exchange upon SRC3 addition, compared to PR-A alone (**Figure 3**). This suggests that SRC3 may induce PR-A dimerization, similar to that observed upon the addition of PRE DNA, as shown in **Figure 2**. Further, reduced exchange was observed at the PR-A NTD when DNA-bound, suggesting direct interactions between the PR NTD and SRC3 (**Figure 3**). Upon addition of PRE to the PR-A:SRC3 complex, increased deuterium incorporation was observed within regions of the PR-A LBD compared to the non-DNA-bound complex (**Figure 3. B**). This is unexpected, as PRE addition should have afforded additional stability to the complex, like that observed for the PR:PRE complexes (**Figure 2**). While increased exchange was observed

in the LBD, neither the dimerization domains nor AF2 (the putative CoR-interaction domain (H3, H4, and H12)) were affected. This indicates that receptor binding either PRE, SRC3, or a combination of the two influences the conformational dynamics of the PR LBD without destabilizing the homodimer.

Similarly, increased deuterium exchange was observed for PR-B:SRC3 complexes, with deuterium exchange increases in the LBD when in the presence of PRE (**Figure S10**), compared to the PR-B:PRE complex shown in **Figure 2**. Overall, PR-B displayed fewer regions of differential deuterium exchange across the protein, compared to PR-A. In the PR-B:SRC3 complex, some protections to exchange were observed in the PR-B NTD; however, not throughout the rest of the protein (**Figure S10**). DNA binding does not seem to affect the PR-B:SRC3 complex, where few differences are measured between the homodimeric complex with the SRC3-containing complex (**Figure S10**). Taken together, these data suggest that there is a concerted SRC3-mediated deprotection of the LBD when PR is DNA bound, whereas SRC3 binding to PR in the absence of DNA stabilizes each PR domain.

To see how the HDX data would inform protein structural changes, AlphaFold3.0[52] predictions were generated for the unbound and PRE-bound PR:SRC3 complexes. Since AlphaFold3.0 introduces spurious structural order (termed, hallucinations)[53] to intrinsically disordered regions such as the NTD of PR, 25 independent models were generated by repeating the structural prediction five times with random seed values. These models were then examined with HDXer[54] to identify the model that best fit the HDX-MS data. The top models chosen each had average root mean square errors (RMSEs) less than 0.4 (**Figure S11**).

The differences between the top model of non-DNA-bound and DNA-bound PR-A, shown in **Figure 2A**, displays interesting SRC3 binding modalities where SRC3 envelops the PR-A homodimer in the DNA-bound model, but not the non-DNA model. The non-DNA-bound model shows a distinct separation between PR and SRC3, indicating that the main interaction site is the hydrophobic AF2-cleft. In the PR-A:SRC3:PRE model, there is a rearrangement of PR-A compared to the non-DNA-containing PR-A:SRC3 model. The homodimer binds to PRE on one face of the response element DNA, while SRC3 energetically favors binding on the opposite side of the DNA (**Figure 2**). This was repeatedly found for each top-scoring model from unique AlphaFold 3.0 seeds. In the HDX data, PR-A had increases in deuterium exchange within bends and loops of the LBD while the DBD and CTE were protected. These data indicate a simultaneous stabilization of the complex on DNA and increased motility at helical connecting regions (**Figure 2.B Right**). Notably, the hydrophobic AF2 cleft in the LBD also showed increased deuterium incorporation, hinting at increased solvent exposure at that boundary (**Figure 2.B Right**).

The representative AlphaFold models of PR-B and SRC3 suggest a similar binding modality to PR-A, where PR-B interacts with SRC3 on one face in the non-DNA-bound state. When bound to DNA, the best fitting model showed PR-B adopting an elongated structure, with greater N-terminal interactions than those observed with PR-A (**Figure S10**). While the orientation of SRC3 is similar between the two PR isoforms, PR-B seems to enhance the protein-protein interactions through its extended N-terminus (**Figure S10**). These observations

enhance the notion that the N-terminus of PR is important for transcriptional activation through protein-protein interactions, and the additional N-terminal residues of PR-B can enhance DNA-bound stability. The differences between non-DNA-bound and DNA-bound data supports a PR priming mechanism, where DNA generally enhances protein-DNA and protein-protein interactions, and the addition of SRC3 affords additional stability, measured by HDX (**Figure 3, Figure S10**).

To gauge these interactions further, chemical crosslinking was used with DSSO to show protein-protein residue proximity. When non-DNA bound, PR-A and SRC3 have multiple interactions, shown by interprotein crosslinking (**Figure S12**). Overlaying the HDX results onto the crosslinking maps demonstrates that most changes in deuterium exchange were localized to regions containing specific inter- or intraprotein crosslinks (**Figure S12**). The crosslinking data agrees with the HDX data, where deuterium exchange events are induced by SRC3 binding. This was inferred based on the increased uptake regions align with interprotein crosslinks between PR-A and SRC3. While the crosslinks in the PR LBD remain unchanged, the HDX data showed an increase in overall solvent exchange (deprotection). Upon PRE binding, the PR-A LBD to SRC3 crosslinks expand to encompass both the LBD and the DBD (**Figure S12**). Combined, the PR DBD becomes protected from deuterium exchange upon co-binding DNA and SRC3; whereas, the LBD showed increased exchange upon SRC3 and PRE binding.

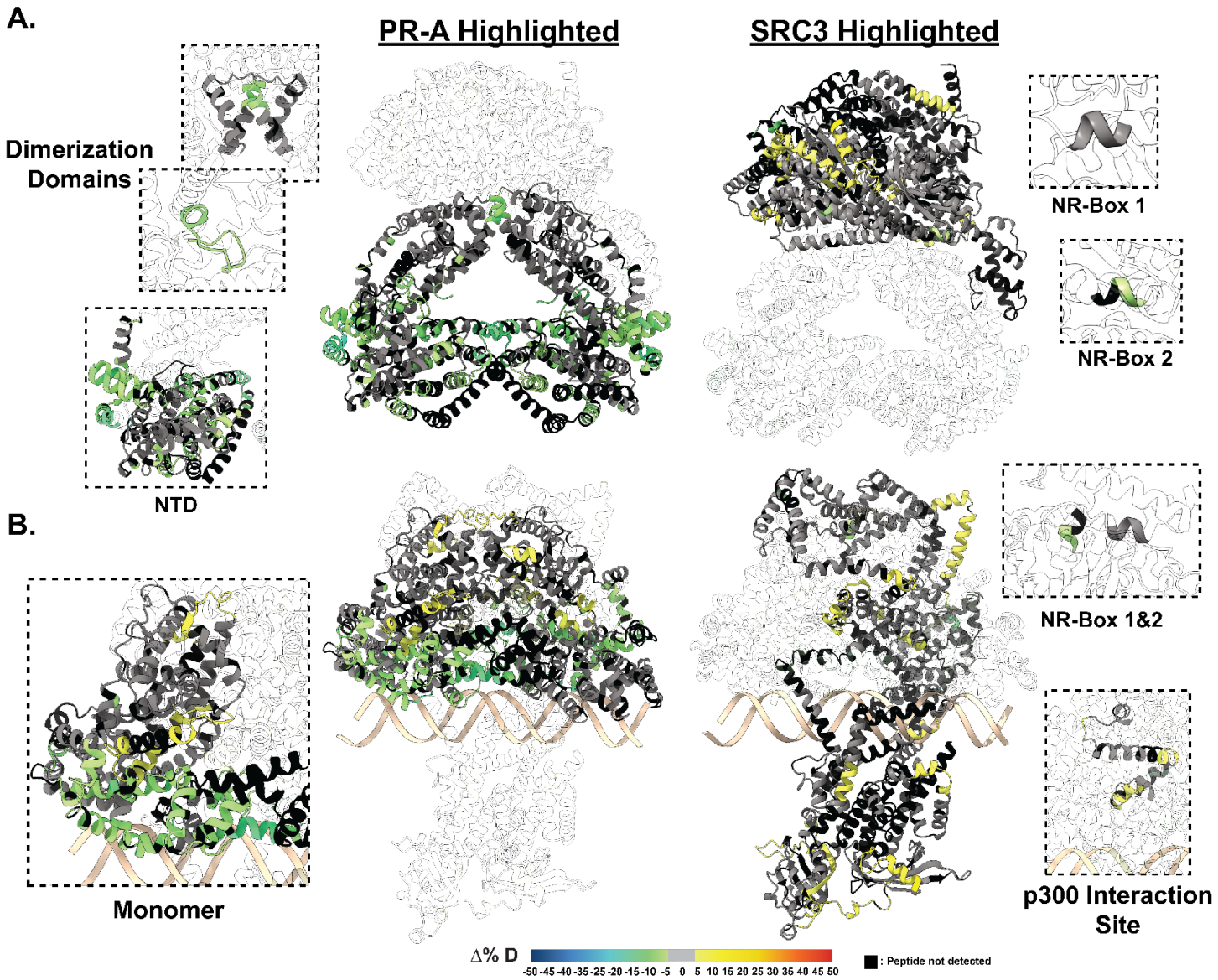

Figure 3. SRC3 induces LBD changes to PR upon PRE addition. ***A. Left*** *HDX overlay (PR-A vs. PR-A:SRC3) mapped onto AlphaFold3.0 model of the PR-A:SRC3 ternary complex with the PR homodimer highlighted. Zoomed-in sections of PR corresponding to the dimerization domains (Amino acids: 720-769 and 438-454) and N-terminal domain (PR-A amino acids 1-476) highlighted with matching HDX overlays.* ***Right.*** *Differential HDX overlay of SRC3 vs. PR-A:SRC3 onto the best scoring PR:SRC3 apo complex with SRC3 highlighted. NR-Boxes 1 and 2 (amino acids 685-689 and 738-742, respectively) blown up to show differential exchange.* ***B. Left*** *HDX overlay (PR-A:PRE vs. PR-A:SRC3:PRE) mapped onto AlphFold3.0 model of PR-A:SRC3:PRE ternary complex with the PR homodimer highlighted. One PR-A monomer is shown as a zoomed-in section.* ***Right.*** *Differential HDX overlay of SRC3 vs. PR-A:SRC3:PRE onto the best scoring PR:SRC3 apo complex with SRC3 highlighted. NR-Boxes 1 and 2 and the p300 interaction site (amino acids 1023-1093) are highlighted to show differential exchange. Black peptide regions correspond to peptides not identified by HDX-MS. Each color represents the percent change in deuterium incorporation (Δ%D), following the scale shown at the bottom.*

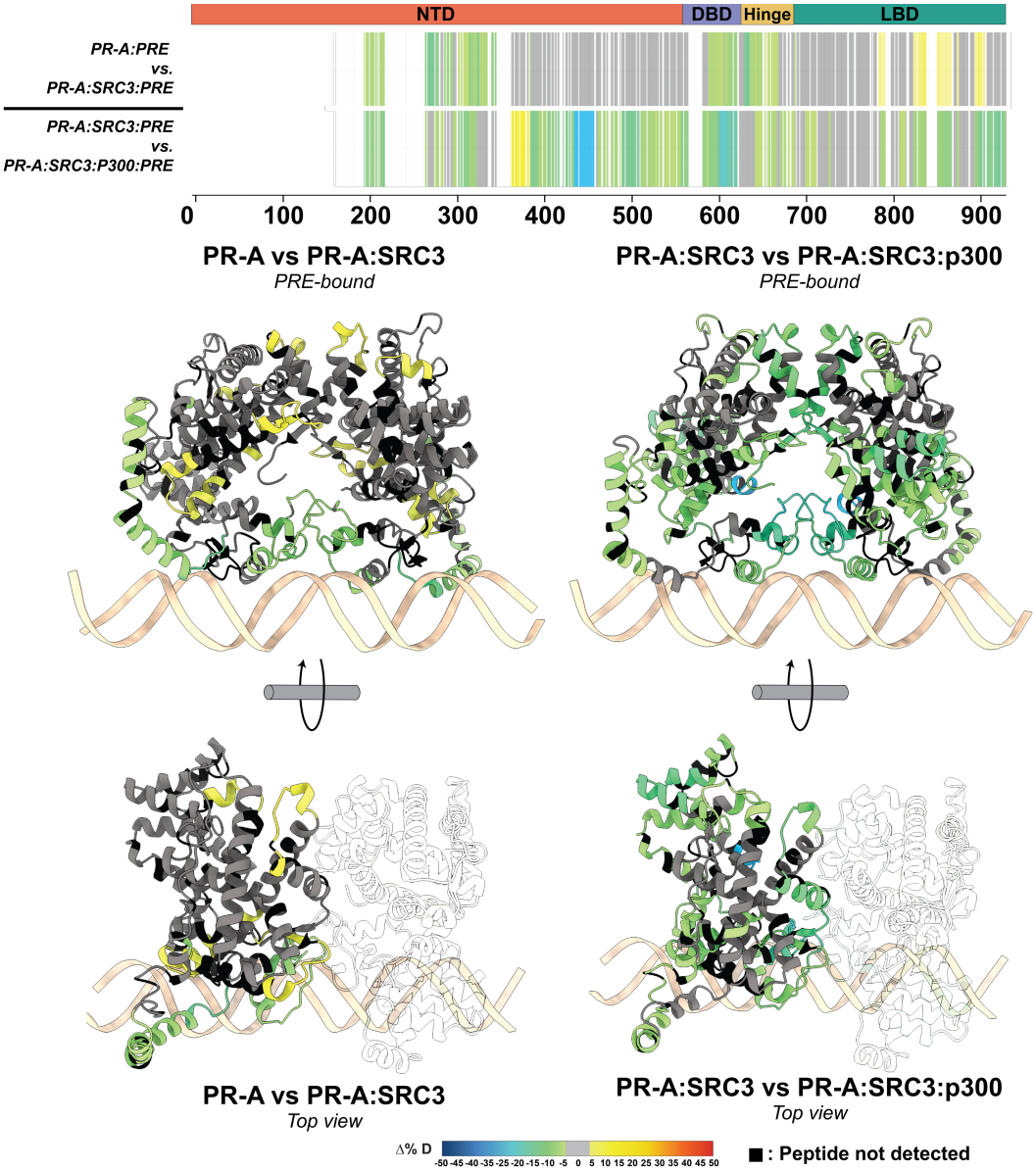

Figure 4. p300 differentially alters the conformational dynamics of PR-A and PR-B within the PR:SRC3:p300 complex. ***Top.*** *Consolidated HDX plots of PR-B showing the differential HDX-MS comparisons within the plot to the left. Changes in deuterium uptake are represented by the rainbow plot shown at the bottom. Common PR domains are highlighted at the top: N-terminal domain (NTD, orange), DNA-binding domain (DBD, purple), Hinge (yellow), and ligand-binding domain (LBD, teal).* ***Bottom.*** *AlphaFold3.0 models of PR from the AF1 to LBD (amino acids 456-933 using PR-B numbering). HDX-MS overlays represent the same experiments as the consolidated views on the top. Each color represents the percent change in deuterium incorporation (Δ%D), following the scale shown at the bottom.Gray overlays indicate no significant changes and black indicates peptides not detected in the HDX-MS experiment.*

After showing that p300 facilitates increased PR:SRC3 interactions and that PR and p300 directly interacted with DSSO crosslinking, PR was re-examined to identify p300 interaction sites using HDX-MS. When p300-bound, there was more than a 10% change in deuterium exchange for both PR and SRC3 (**Figure 3, Figure 5**). These reductions in solvent exchange show that p300 strengthens the ternary complex, whether through direct PR-p300 interactions or strengthening the PR-SRC3 interaction. This behavior was only measured with PR-A, where we found a concerted shift from deprotected to protected regions in the PRE-containing complexes (**Figure 5**). The previously deprotected sites in the PR-A:SRC3:PRE complexes become protected once p300

is added to the system (**Figure 5**). This points to increased complex stability for the PR-A complexes. Interestingly, this is only seen with the A isoform, and PR-B is largely unchanged when p300 is added. Considering that we observe changes to SRC3 when we have PR-B, SRC3, and p300, it suggests that complex formation is not dependent on direct PR-B interactions.

Structural proteomics identifies SRC3 and p300 NR-box utilization for PR isoforms

Within SRC3 are conserved domains known as nuclear receptor (NR) boxes. NR-boxes are sequences that promote nuclear receptor binding with a motif of LXXLL. In the case of PR-SRC3 interactions, these indicate a potential PR binding site. For SRC3, there are three separate NR boxes where PR has the potential to bind (amino acids 685-689, 738-742, and 1057-1061). It is unknown, though, which or how many of these are necessary for the PR-SRC3 interaction. Prior data has identified PR utilization of a combination of NR-Box 1 and 2 for SRC1-mediated activation,[55-57] yet this has not been assessed for SRC3. Using HDX-MS, deuterium exchange profiles can be monitored for multiple proteins within a singular experiment. Solvent exchange was measured for both PR and SRC3 for each differential HDX-MS experiment, similar to the exchange measured with PR. Differential HDX-MS experiments showed decreased deuterium exchange at NR-box 2 upon PR addition and non-significant (see: Methods – Data Rendering) decreases in NR-box 1 (**Figure 5**). Interestingly, at NR-box 3, slight increases in solvent exchange were observed, suggesting reduced stability or structural arrangement at this region (**Figure 5**). These data suggest that NR-box 2 is initially utilized by PR, NR-box 1 is utilized to a lesser extent, and the third NR-box remains unbound in both the PR apo and PRE-bound state.

Upon p300 addition, all NR-boxes were protected in the PR:SRC3:p300 and PR:SRC3:p300:PRE differential experiments, including NR-Box 3 (**Figure 5**). From the deuterium uptake curves of representative peptides in each NR-Box region, a nearly two-fold difference in the deuterium uptake was measured for NR-Box 3 (**Figure 5**). Since NR-box 3 was not protected in the absence of p300 in the PR:SRC3 complex, this observation implies that p300 directly binds NR-box 3. This is further supported by the crosslinking data, where PR formed crosslinks near NR-boxes 1 and 2 of SRC3 and p300 crosslinks with the third NR-box in SRC3 (**Figure S13**). In addition, p300 induced widespread protection throughout PR and SRC3. Taken together, it is clear that p300 stabilizes both PR and SRC3 in both the absence and presence of DNA.

Similar comparisons were made using PR-B, instead of PR-A, which showed different deuterium exchange compared to PR-A. In the SRC3 ± PR-B experiments, no protections from solvent exchange were observed in any NR-Box. However, solvent exchange increased in NR-Boxes 2 and 3 upon PR binding, regardless of PRE presence. Increases to exchange in NR-Box 1 were only observed in the presence of PRE. Upon p300 binding, there was exchange protection in each NR-box, different than the sequential binding seen with PR-A (**Figure 5**). The other SRC3 domains, though, have a similar protection pattern to PR-A where the bHLH, PAS, CREBBP interaction domain, and putative acetyltransferase domains were protected only in the presence of p300, most likely indicating direct p300 binding at those regions. Like PR-A, PR-B forms crosslinks within NR-boxes 1 and 2, whereas NR-box 3 only contains crosslinks between SRC3 and p300 (**Figure S13**).

To further investigate the necessity of each NR-box for PR activation, promoter:reporter assays were used in conjunction with site-directed mutagenesis to assess the impact on PR transcriptional output. PR transcriptional response was indirectly measured using a PRE-firefly luciferase reporter plasmid[58] to compare WT and NR-box mutations. Mutating SRC3 NR-Box 2 from LXXLL to LXXAA resulted in reduced PR response (**Figure S14**). Changing other NR-Box sequences to LXXAA at either Box 1 or Box 3 did not result in reduced PR activity (**Figure S14**). However, combination mutants: NR-boxes 1+2 and 1+3 reduce PR activity. The SRC3 Box 2+3 mutant increases overall activity (**Figure S14**). Surprisingly, the mutation of all three NR-boxes did not show any significant differences between WT PR-B and WT-SRC3, suggesting a potential compensatory mechanism. These results suggest NR-box 2 is an important PR interaction site for transcriptional response, and combination mutants involving NR-Box 1 are deleterious to PR activity. These assays were repeated with PR-A, but the results were inconclusive due to intrinsically reduced transcriptional response (**Figure S14**).

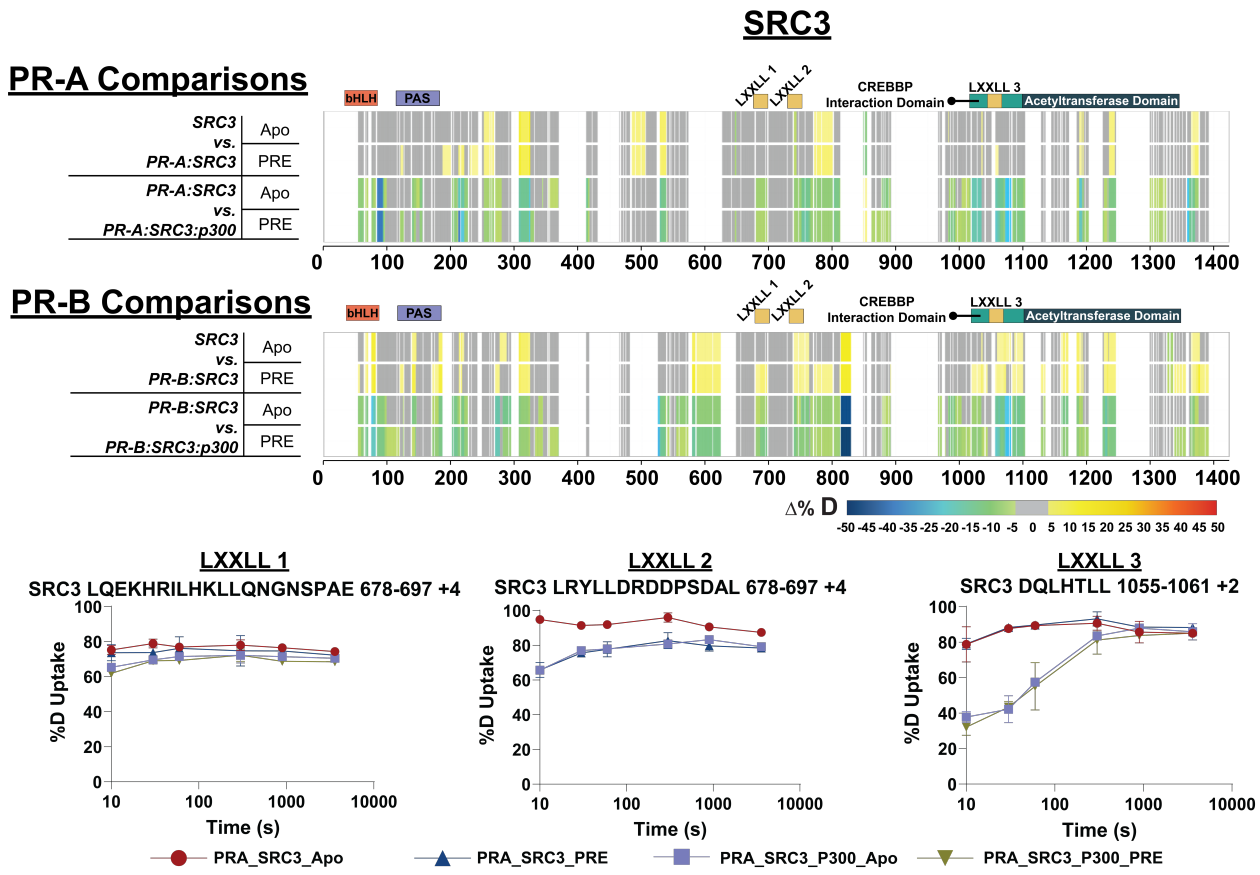

Figure 5. PR-A and PR-B differentially interact with SRC3 and are stabilized by p300 addition. ***Top.*** *Consolidated differential HDX-MS results for SRC3, comparing the changes induced by PR-A and p300 binding in the presence and absence of PRE DNA.* ***Middle.*** *Consolidated HDX-MS plot of SRC3 exchange, with PR-B comparisons in the same order as PR-A. The motifs highlighted are the following: bHLH (orange), PAS (purple), LXXLL motifs (yellow), CREBBP Interaction domain (teal), and acetyltransferase domain (dark blue). Each color represents the percent change in deuterium incorporation (Δ%D), following the scale shown at the bottom.Gray overlays indicate no significant changes and black indicates peptides not detected in the HDX-MS experiment.* ***Bottom.*** *Selected deuterium uptake plots for peptides that contain LXXLL motifs 1, 2, and 3. The % uptake indicates the deuterium uptake over time for the PR-A, PR-A:SRC3, and PR-A:SRC3:p300 HDX experiments.*

Previous data has shown that sequential addition of SRC3 and p300 increases PR transcriptional response. However, based on the crosslinking results of the PR:SRC3:p300 ternary complex (**Figure S13**), direct PR-p300 interactions were investigated by XL-MS. In the absence of SRC3, PR and p300 formed crosslinks, indicating direct protein-protein interactions (**Figure 6**). Crosslinks to both the N-terminus and C-terminus show that there are multi-pronged PR-p300 interactions without SRC3. These included crosslinks to the p300 NR-boxes, bromodomain, and core acetyltransferase regions.

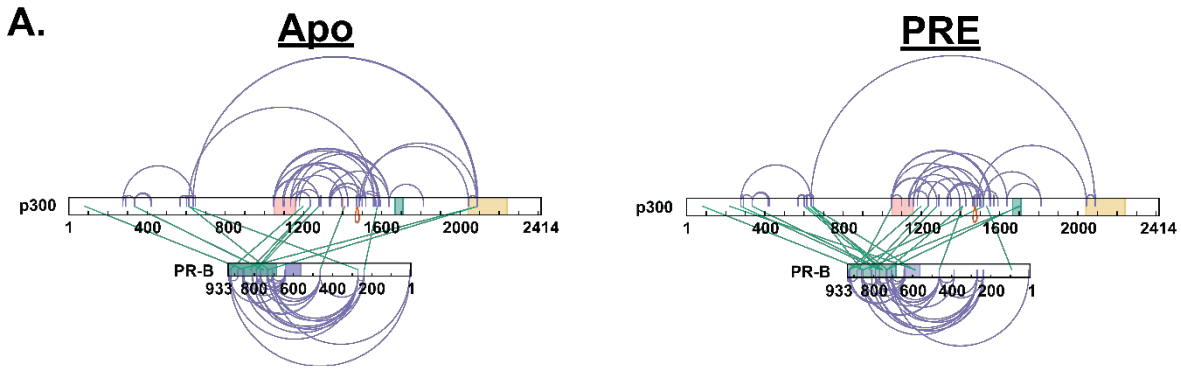

Figure 6. XL-MS shows p300 directly interacts with PR. ***A.*** *Crosslinking results from PR-B:p300±PRE experiments. Purple: intraprotein crosslinks, green: interprotein crosslinks. PR highlighted domains: DBD (purple) and LBD (green). p300 highlighted domains: bromodomain (pink), zinc finger domain (green), and NCOA2-interaction domain (yellow).*

RU486-antagonism reorganizes PR:SRC3 and PR:SRC3:p300 protein complexes

Upon comparing the R5020-bound states of PR, the organization of these complexes with PR-A or PR-B bound to the progestin antagonist, RU486, was investigated. Using the same procedures for purification for PR bound to agonist, except for addition of RU486 to insect cell cultures during expression, purified PR products were of similar yields, concentrations and purity as with PR-agonist (data not shown). As determined by SEC-MALS, both PR-A and PR-B bound to RU486 showed monomeric MW distribution in the absence of DNA (**Figure S15**). With addition of DNA, both PR isoforms assembled as a DNA complex with an experimentally determined MW within the expected theoretical for PR-A and PR-B dimers **(Figure S15, Table S1).** This behavior of purified PR bound to RU486 is consistent with previous studies demonstrating RU486 promotes efficient PR dimerization and binding to PRE DNA.[3, 59, 60] Biochemical experiments with PR bound to RU486 have shown that the C-terminal tail of the LBD adopts a distinct conformation from that of agonist bound PR[61, 62] and X-ray crystallography of PR LBD bound to RU486 results in a displacement of helix 12 in multiple potential conformations that may interfere with formation of an AF2 interaction surface for binding LXXLL motifs of Co-activators.[28] X-ray crystallography of the PR LBD bound to antagonists related to RU486 further show a displacement of helix 12 from agonist conformation and differential binding of a peptide from the corepressor SMRT.[63] Studies to date have not explored the influence of RU486 on interactions of PR and CoRs, each as full length proteins to explore alterations in interaction surfaces outside of the LBD.

XL-MS and HDX-MS analysis XL-MS and HDX-MS analysis demonstrates these proteins interact, but they display a different binding modality than agonist-bound protein. In the agonist-bound complex, PR-SRC3 crosslinks group near the C-terminus of both proteins. However, when PR is RU486-bound, the enriched crosslinks shift from a C-terminal region to an N-terminal region (**Figure 7**). This suggests that the proteins can interact, though not in an unexpected manner. Interestingly, crosslinks were retained between PR and SRC3 in the antagonist-bound ternary complex, but additional crosslinks to p300 were found, suggesting all three proteins can still interact when antagonist-bound. Comparing the interaction sites between R5020-bound and RU486-bound protein showed a concerted loss of crosslinking between PR and p300 at the C-terminus (**Figure 7**). This may be indicative of a transition from an active to inactive state for PR:SRC3:p300 driven transcription.

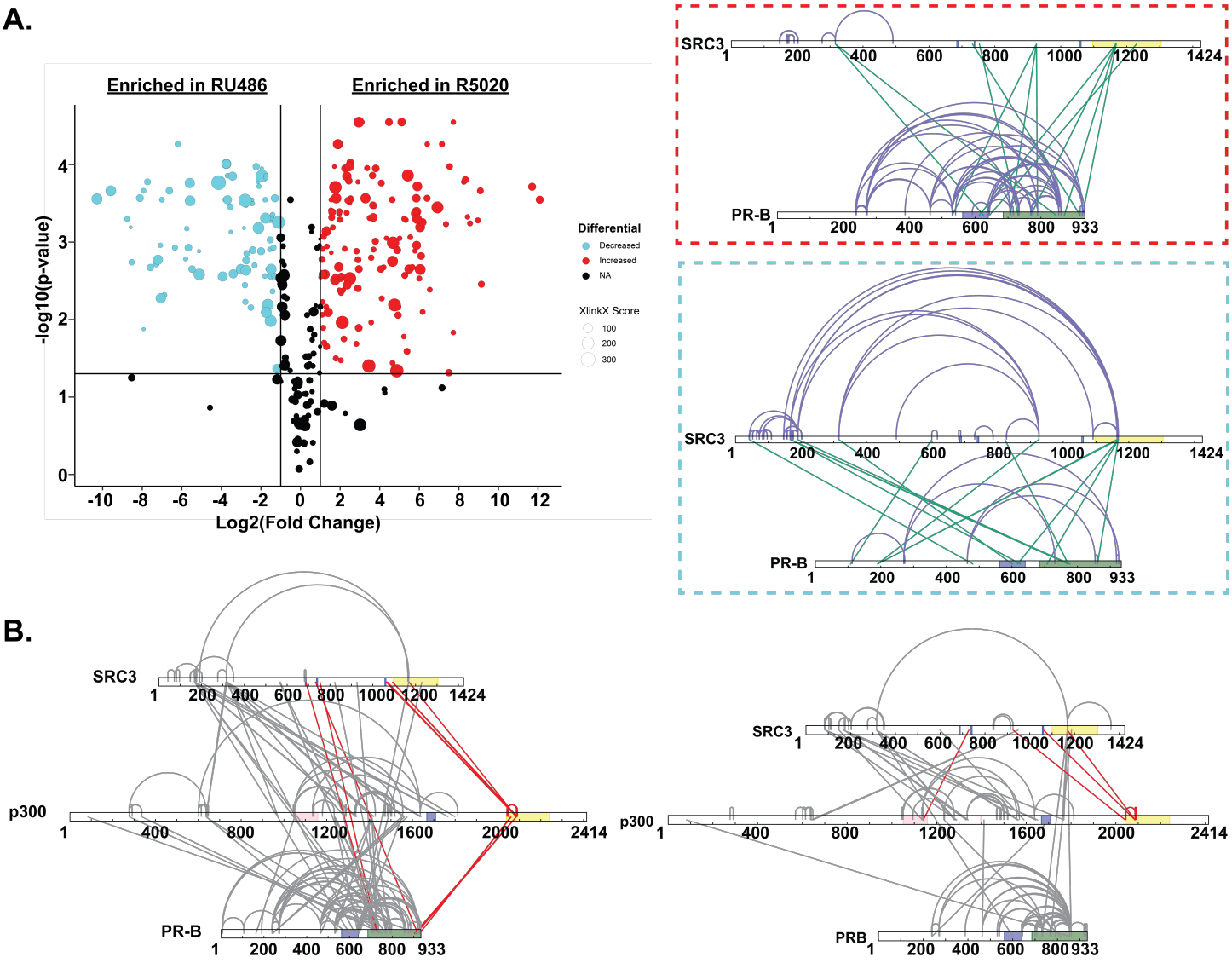

Figure 7. RU486 antagonism rearranges PR-SRC3-p300 interactions. ***Top.*** *Plotted differential crosslinks in PR:SRC3 experiments, comparing R5020-specific (agonist, red) and RU-486-specific (antagonist, blue) crosslinks. Crosslinks represented by circles with corresponding XlinkX scores as point size.* ***Top.Red.*** *XlinkX view of R5020-specific crosslinks in differential PR:SRC3 experiments.* ***Top Blue.*** *XlinkX view of RU486-specific crosslinks in differential PR:SRC3 experiments.* ***B.*** *All validated R5020 (left) and RU486 (right) crosslinks for differential PR-B:SRC3:p300 ± PRE experiments. Crosslinks highlighted in red show notable differences in*

PR:SRC3:p300 interactions between PR ligands. Defined domains are as follows: PR - DBD (purple) and LBD (green); SRC3 – NR-boxes (purple) and histone acetyltransferase domain (yellow); p300 - bromodomain (pink), zinc finger domain (green), and NCOA2-interaction domain (yellow).

HDX-MS was applied to investigate the backbone dynamics of each protein. Different than the R5020-bound complexes, the presence of antagonist significantly reduced deuterium exchange, specifically in all of the PR ± PRE experiments (**Figure S16**). However, the sequential addition of co-regulators showed an expected solvent exchange profile, compared to the PR ± PRE experiments. Based on this, comparisons were made between the larger ternary complexes. Interestingly, regions of protection were observed for the larger ternary complexes with both PR-A and PR-B when comparing the presence of DNA (**Figure 8**). The differential deuterium uptake was very similar to that seen with agonist (R5020)-bound PR (**Figure 3**). Protected regions were localized to the DBD, CTE, and LBD, all regions known to interact with DNA and CoRs. Specifically, portions of the AF1 and AF2 cleft had reduced deuterium exchange (**Figure 8**), which is a hallmark of CoR binding. Prior work had shown that AF1 and AF2 have distinct roles in CoR interactions.[28, 64-67] This suggests that when antagonist-bound, PR can still associate with co-activators: SRC3 and p300.

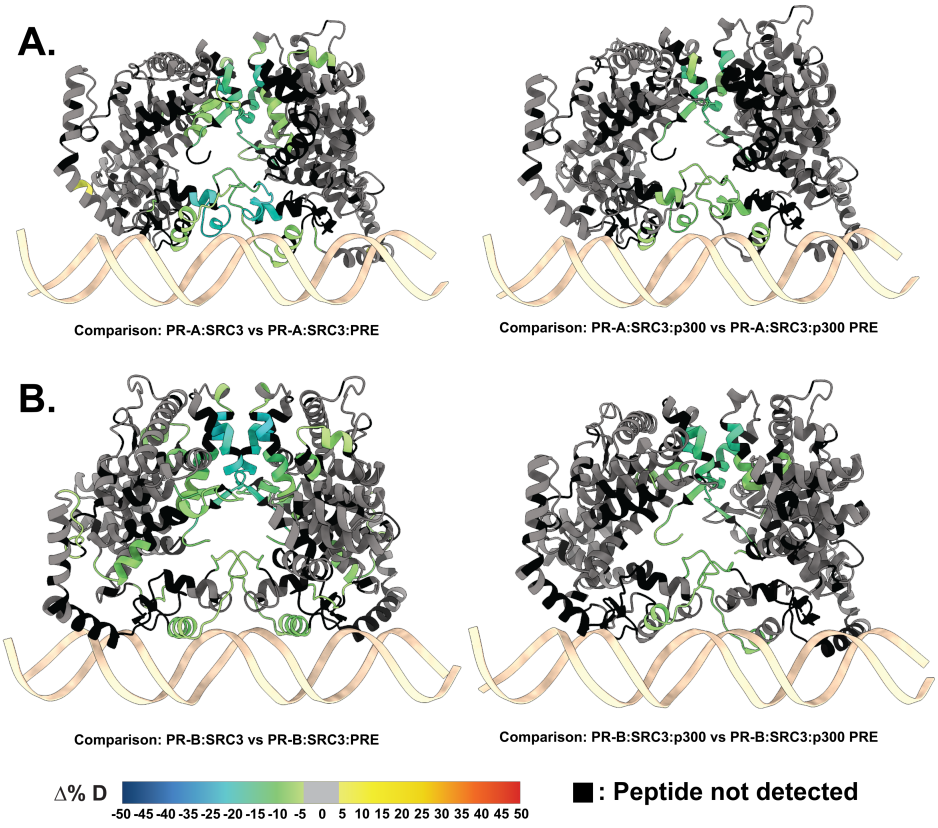

Figure 8. RU486-bound PR has reduced deuterium exchange upon CoR binding. ***A.*** *PR models of AF1 to C-terminus (amino acids 456-933) with PR-A HDX overlays, corresponding to the comparisons shown beneath them.* ***B.*** *PR models of the AF1 to C-terminus with corresponding PR-B HDX overlays labeled beneath. Each color represents the percent change in deuterium incorporation (Δ%D), following the scale shown at the bottom.Gray overlays indicate no significant changes and black indicates peptides not detected in the HDX-MS experiment.*

Discussion

Steroid nuclear receptors (SR) are hormone-responsive transcription factors that exhibit remarkable functional diversity in mediating cell and target gene specific responses, largely driven by conformational dynamics of the receptor that enables it's binding of unique subsets of transcriptional CoRs and DNA response elements. PR is the main target of progestogens that are widely used clinically and is expressed as two protein isoforms, an N-terminal truncated PR-A and full-length PR-B and each have distinct physiological roles dependent on the cell or tissue type. In general PR-A is a weaker transcriptional activator than PR-B, and can act to attenuate the activity of PR-B. Both isoforms are typically co-expressed in equal proportions in most normal tissues. However, PR-A to PR-B ratios have been reported to be highly variable in pathological conditions. Mechanistic basis for differences in activity of the isoforms is not well defined but is generally thought to be due to isoform-specific structural conformations and differential CoR interactions. Despite the general understanding of the mechanism of PRs action in physiology and pathophysiology, the full therapeutic potential of has not been utilized. This, in part, is due to lack of knowledge about the structural dynamics of two PR isoforms, PR-A and PR-B. To fully understand the biological functions of PR, it is imperative to know how DNA-bound receptor recruits transcriptional CoR complexes through protein–protein interactions involving CoRs. Recent low-resolution cryoEM structure of PR-B gave some clues about how such complexes may be formed; however, the missing atomic-level structural details limited the understanding of interactions between PR-B and its CoRs used in that study. Moreover, structural understanding of PR-A and PR-A:CoR complexes is completely lacking. One of the associated problems in solving high-resolution structural analyses has been generation of stable PR:CoR complexes with or without DNA-bound. Our studies clearly demonstrate generation of stable protein complexes with expected stoichiometry. This paved the way not only for carrying out structural dynamic studies of PR isoforms and their interactions with CoRs with or without bound to DNA but also for future structural studies for which finding a stable complex has been challenging.

Here, XL-MS and HDX-MS were used to make solution-phase structural measurements of amino acid distance constraints between protein components and to probe conformational dynamics of PR-A and PR-B in complex with DNA and CoRs. As expected, our results show both PR-A and PR-B binding to DNA as dimer. It has been hypothesized that DNA binding induces compact structure particularly in the ID NTD and other structurally flexible regions. Our HDX-MS data shows much less perturbations in the PR-B NTD but not as much in PR-A suggesting that DNA binding induces stable conformation in ID NTD of PR-B, which possess much larger ID conformation compared with PR-A. Stabilization of NTD structure maybe playing an important role in mediating higher PR-B transactivation activity as has been the case. Further, differential N- and C- terminal interactions in the presence or absence of DNA suggest that there are structural rearrangements in the full-length receptor, which is dependent on PR dimerization and DNA binding. These are novel findings and provide much needed information regarding structural dynamics of PR and would likely apply to other members of SR family.

Reduced perturbations observed throughout PR-A following the binding of SRC-3 particularly in the PR dimerization region suggests that that SRC3 may induce PR-A dimerization without the addition of PRE DNA.

Further stabilization of PR NTD and destabilization in the LBD upon DNA binding suggests direct interactions between the PR NTD and SRC3. It is interesting that perturbations observed in the LBD are not affecting either the LBD dimerization or AF2 regions suggesting that these conformational changes are not destabilizing the PR dimerization rather influencing the conformational dynamics of the PR LBD. Based on these observations, it can be hypothesized that such conformational dynamic changes may be important in providing PR-A surfaces for interactions with other CoRs as well as facilitate the process of the exclusion or inclusion of specific CoRs in the complex, a phenomenon commonly adopted by SRs when moving from one PRE site to another one in the genome. The differential effects on PR-A vs PR-B isoforms using both AlphaFold3.0 model fitting and cross-linking data not only support these observations but also suggests that conformational dynamics in the complex is isoform dependent. This finding may provide a mechanistic basis for differences in the activities of the two receptor isoforms.

In summary the computational models presented indicate that PR:SRC3:p300 complexes have unique structures specific to different isoforms, a conclusion supported by structural proteomic data. The experimental results presented reveal a sequential priming mechanism for progesterone receptor (PR) involving several key findings. When SRC3 binds to the PR-PRE complex, it leads to increased solvent exchange within the ligand-binding domain (LBD) of PR, suggesting that SRC3 induces conformational changes that prepare PR for interaction with p300. P300 further interacts with both the N- and C- termini of PR, positioning its HAT domain in close proximity to DNA and chromatin. Additionally, PR binds to SRC3's NR boxes 1 and 2, while p300 binds to NR box 3, indicating a specific order of complex assembly. Surprisingly, and contrary to classical models, SRC3 and p300 remain associated with PR when bound to antagonist, although the orientation of the complex differs from that observed with an agonist suggesting antagonist driven rearrangement of the transcriptional complex. Collectively, the findings presented here elucidate how SRC3 and p300 interact with PR-A and PR-B, influencing its function and conformation.

Methods

Materials.

Oligonucleotides (Sigma-Aldrich). 32 mer progesterone response element (PRE) dsDNA sequences: Sense: 5’-CATCTTTGAGAACAAACTGTTCTTAAAACGAG-3’; Antisense: 5’-CTCGTTTTAAGAACAGTTTGTTCTCAAAGATG-3’. Sigma-Aldrich provided Disodium hydrogen phosphate (Na_2HPO_4) (S9763), Sodium Chloride (NaCl) (S9888), Urea (51456), Benzonase (9025-65-4) and 2-Mercaptoethanol (2ME) (M3148). Fisher Scientific provided Glycerol (BP229-4), and Biotin (B0463). Hampton Research provided TCEP Hydrochloride (50-093-0). Invitrogen provided UltraPure™ 0.5M EDTA (15575020) and SYPRO Gel filtration standard (S6650). BIO-RAD provided unstained protein standard (1610363) and Gel

Filtration Standard (1511901). Thermo Fisher provided Zeba™ Spin Desalting Columns 7K MWCO 0.5 mL (89882) and Disposable PES Bottle 0.2uM Top Filters (166-0045).

Plasmids.

Progesterone receptor protein-expression plasmids, pRP[Exp]-EGFP/PuroEF1A>hRluc(ns):P2A:hPGR[NM_000926.4] (co)* and pRP[Exp]-EGFP/PuroEF1A>hRluc(ns):P2A:hPGR[NM_001202474.3] (co)*, were constructed by VectorBuilder. Their respective vector IDs are VB230919-1497uvg and VB230919-1498ukn, which can be used to retrieve detailed information about the vector on vectorbuilder.com. Progesterone response plasmid, 4X PRE TK luc, was a gift from Renee van Amerongen[58] (Addgene plasmid # 206159 ; http://n2t.net/addgene:206159 ; RRID:Addgene_206159).

Protein expression.

Human PR-A, PR-B, SRC3, and p300 as full-length open reading frame DNA were each synthesized with optimal codon usage for insect cells with an in-frame Strep II tag (WSHPQFEK/G) and a glycine spacer at the amino-terminus and inserted into pFastBac1 transfer vectors (Epoch Life Sciences, Houston, TX). Recombinant bacmids were generated and expanded in Spodoptera frugiperda (Sf9) cell cultures and viral titers were determined by plaque assays as previously described (Kumar R et J biol Chem. 288:30285-299, 2103; Wardell SE et al Mol Cell Biol. 25:8792-8808, 2005). Multiple 0.5 liter cultures of SF9 cells were infected with recombinant virus at an MOI of 2.0 and incubated for 48 hour at 27C in oxygenated spinner vessels. For cells expressing PR-A or PR-B, the progestin agonist R5020 or antagonist RU486 was added to Sf9 cell cultures at 250nM for 24 hours post-infection. Cells were collected and centrifuged 1500x g for 10min and pellets were washed once PBS by resuspension and centrifugation. Cell pellets were flash frozen and stored at -80C.

Protein purification.

Cells (from 2x 500ml cultures) were resuspended in 50ml of lysis buffer (50mM Na_2HPO_4, pH 8.0, 500 mM NaCl, 5% Glycerol, 1M Urea, 1mM EDTA, 1mM 2ME), supplemented with protease inhibitor tablets (leupetin,aprotinin, bactracin and PMSF) and submitted to Teflon-glass homogenizer for 8 strokes at 1.5 speed in the cold room. The homogenate was treated with 1.2 units/ml of benzonase nuclease or 1 hour at 4C then passed 3 times through an 18G needle followed by a 25G needle. The lysate was centrifuged twice for 1 hour at 50,00 xg and the resulting supernatant was filtered using 0.2uM disposable filters. Purification was performed on AKTA Pure™ 25 at 4 °C while monitoring conductivity and UV. A 1ml StrepTrap XT prepacked Hi-Trap chromatography column (Cytiva) was equilibrated with lysis buffer for 10 column volumes (CV), and after loading the cleared cell lysate, the column was washed for 30 CV with equilibration buffer and then eluted with equilibration buffer containing 40mM biotin. Eluted fractions (1 mL) were collected and analyzed by

Coomassie Blue-stained 4-15% gradient SDS-PAGE gel. Fractions containing proteins of interest were pooled and concentrated to 1-2ml by an Amicon ultracentrifugal device with a 10,000 MW cutoff (A280<4.0). Proteins were further purified by a preparative size exclusion chromatography (SCE) column (HiLoad 16/600 Superdex 200pg), degassed and equilibrated in SEC buffer (20 mM Hepes, pH 7.5, 200 mM NaCl, 5% Glycerol, 1M Urea and 1 mM TCEP). Elution fractions (1 mL) were collected and analyzed by Coomassie Blue-stained 4-15% gradient SDS-PAGE gels and peak fractions were concentrated as above. Concentrations of purified protein products were by determined by Nanodrop absorbance at 280/260nm, calculation of extinction coefficient, and by comparison of purified bands on Coomassie Blue-stained 4-15% SDS-PAGE gel with a standard curve of know amounts of unstained protein markers. Aliquots (50-100uL) of purified protein were snap frozen in liquid nitrogen and stored at -80°C for up to 3-4 months and samples were used only one time after thawing.

Analytical SEC.

All procedures were conducted at a temperature range of 0°C to 4°C.. Protein samples (50 µL each) were injected using a capillary syringe into a 50 µL loop and fractionated over a Superdex 6 Increase 5/150 GL column. The column was equilibrated with degassed SEC Buffer (20 mM Hepes, pH 7.5, 200 mM NaCl, 5% Glycerol, 1 M Urea, and 1 mM TCEP) as well as degassed SEC buffer without Urea (20 mM Hepes, pH 7.5, 200 mM NaCl, 5% Glycerol, and 1 mM TCEP). Columns were calibrated using Gel Filtration Standards.

Differential Scanning Fluorimetry (DSF).

The thermal stability of SII tagged purified proteins were measured by differential scanning fluorimetry (DSF) using the CFX96 Touch Real-Time PCR Detection System (BIO-RAD) instrument. Fluorescence monitoring was performed at 10°C–95°C at a rate of 0.5◦C/S. Each reaction contained 1uL 500x SYPRO™ Orange gel stain, 4ug purified protein and storage buffer which brought the reaction volume to 20uL. All samples were scanned 3 times as technical replicates. Melting temperatures (Tm) were estimated using the Bio-Rad CFX Maestro computer program by fitting the Boltzmann sigmoidal curve to the normalized data and values are average of 3 replicates with standard error of the mean.

Size Exclusion Chromatography-Multi-Angle Light Scattering (SEC-MALS).

Data were collected using a Dawn Ambient light scattering instrument equipped with a 661 nm laser (Wyatt). The whole system is linked to an HPLC system with UV absorbance detection at 280 nm (Agilent) and an Optilab (Wyatt) for differential refractive index (dRI) measurements. Approximately 20 to 100 µg of proteins (p300, SRC3, PR-A (agonist R5020 or antagonist RU486), PR-B (R5020or RU486) or DNA alone or in complexes were injected and flowed through a Superose 6 increase column (Cytiva). Data was analyzed using the Astra software (Wyatt). BSA sample was also run as a calibration control and to obtain the dn/dc values in the different buffer conditions. The buffer was 20 mM Hepes, 50mM NaCl, 5% glycerol, 1 mM TCEP, with or without 1 M Urea, pH 7.5. Figures were plotted using the Origin software. Standard errors shown were 5% of the calculated MW.

Hydrogen-Deuterium Exchange Mass Spectrometry

Peptide identification

Peptides were identified using MS/MS experiments performed on a QExactive (ThermoFisher Scientific, San Jose, CA) over a 70-min gradient. Product ion spectra were acquired in a data-dependent mode, and the five most abundant ions were selected for the product ion analysis per scan event. For peptide identification, the MS/MS *.raw data files were analyzed on Sequest (version 2.3, Matrix Science, London, UK). The maximum number of missed cleavages was set to four with a mass tolerance of ±0.6 Da for precursor ions and ±10 ppm for fragment ions. Oxidation to methionine was selected for variable modification. An in-house combination FungalXIII/Pepsin column coupled at an equimolar ratio was used for digestion, with non-specific digestion used in the search parameters. Only peptides with an FDR<1% were used in the dataset, and peptides were filtered for duplicates.

Continuous labeling

Experiments with continuous labeling were carried out on a fully automated system (CTC HTS PAL, LEAP Technologies, Carrboro, NC; housed inside a 4°C cabinet) as previously described[35] with the following modifications: For differential HDX, protein-protein complexes were generated by sequential protein addition, where each protein would incubate for 15 minutes at 4°C before sequential addition of the next protein. The final incubation was carried out in the sample plate for 30 minutes before the experiment started (1-hour total incubation time from final protein addition). The reactions (5 µL) were mixed with 20 µL of deuterated (D2O-containing) buffer [20 mM Hepes, 200 mM NaCl, 1M Urea, 1 mM TCEP, and 5% glycerol (pD 8.4)] and incubated at 4°C for 0, 10, 30, 60, 900, or 3600 s. Following on-exchange, unwanted forward- or back-exchange was minimized, and the protein complex deuteration was stopped by the addition of 25 µL of a quench solution [20mM NaH_2PO_4 and 1% TFA (pH 2.5)] before immediate online digestion and data acquisition.

HDX-MS analysis

Samples were digested through an immobilized fungal XIII/pepsin column (1 to 1 ratio, prepared in-house) at 50 µL/min [0.1% (v/v) TFA at 4°C]. The resulting peptides were trapped and desalted on a 2 mm-by-10 mm C8 trap column (Hypersil Gold, ThermoFisher Scientific). The bound peptides were then gradient-eluted [4 to 40% (v/v) CH_3CN and 0.3% (v/v) formic acid] on a 2.1 mm-by-50 mm C18 separation column (Hypersil Gold, ThermoFisher Scientific) for 5 min. Sample handling and peptide separation were conducted at 4°C. The eluted peptides were then subjected to electrospray ionization directly coupled to a high-resolution Orbitrap mass spectrometer (QExactive, ThermoFisher Scientific).

Data rendering

The intensity-weighted mean m/z centroid value of each peptide envelope was calculated and subsequently converted into a percentage of deuterium incorporation. This is accomplished by determining the observed averages of the undeuterated and fully deuterated spectra using the conventional formula described elsewhere.[33] The fully deuterated control, 100% deuterium incorporation, was calculated theoretically, and corrections for back-exchange were based on an estimated 70% deuterium recovery while accounting for 80% final deuterium concentration in the sample (1:5 dilution in deuterated buffer). Statistical significance for the differential HDX data is determined by an unpaired t-test for each time point, a procedure that is integrated into the HDX Workbench software.[68]

The HDX data from all overlapping peptides were consolidated to individual amino acid values using a residue averaging approach. For each residue, the deuterium incorporation values and peptide lengths from all overlapping peptides were assembled. A weighting function was applied in which shorter peptides are weighted higher than longer peptides. Each weighted deuterium incorporation value was then averaged by incorporating this weighting function to produce a single value for each amino acid. The initial two residues of each peptide, as well as prolines, were omitted from the calculations. This approach is similar to that previously described.[69] Deuterium uptake for each peptide is calculated as the average of %D for all on-exchange time points, and the difference in average %D values between the unbound and bound samples is presented as a heatmap with a color code given at the bottom of each figure (warm colors for deprotection and cool colors for protection). Peptides are colored by the software automatically to display significant differences, determined either by a greater than 5% difference (less or more protection) in average deuterium uptake between the two states or by using the results of unpaired t-tests at each time point ($P < 0.05$ for any two time points or $P < 0.01$ for any single time point). Peptides with nonsignificant changes between the two states are colored gray. The exchange of the first two residues for any given peptide is not colored. Each peptide bar in the heatmap view displays the average Δ %D values, associated SD, and the charge state. In addition, overlapping peptides with a similar protection trend covering the same region are used to rule out data ambiguity. Outputs from data rendering were transferred to ChimeraX (version 1.8) for generating data overlays onto the generated models

These data have been deposited to the ProteomeXchange Consortium via the PRIDE[70] partner repository with the dataset identifier PXDXXXXXX for continuous labeling HDX-MS experiments.

Crosslinking Mass Spectrometry.

Sample preparation

For DSSO (ThermoFisher Scientific) cross-linking reactions, individual protein and protein-protein complexes were diluted to 5 μM in cross-linking buffer [20 mM Hepes (pH 7.5), 200 mM NaCl, 1M Urea, 1 mM TCEP, and 5% glycerol] and incubated for 30 min at room temperature before initiating the cross-linking reaction. DSSO cross-linker was freshly dissolved in the cross-linking buffer to a final concentration of 150 mM before being

added to the protein solution at a final concentration of 3 mM. The reaction was incubated at 25°C for 45 min and then quenched by adding 1 µL of 2.0 M tris (pH 8.0) and incubating for an additional 10 min at 25°C. Control reactions were performed in parallel by adding DMSO instead of crosslinker. All cross-linking reactions were carried out in three replicates. The presence of cross-linked proteins was confirmed by comparing to the no-crosslink negative control samples using SDS-PAGE and Coomassie staining. The remaining cross-linked and non-crosslinked samples were separately pooled and precipitated using cold acetone extraction. Dried protein pellets were resuspended in 12.5 µL of resuspension buffer [50 mM ammonium bicarbonate and 8 M urea (pH 8.0)]. ProteaseMAX (Promega, V5111) was added to 0.02%, and the solutions were mixed on an orbital shaker operating at 600 rpm for 5 min. After resuspension, 87.5 µL of digestion buffer [50 mM ammonium bicarbonate (pH 8.0)] was added. Protein solutions were digested using trypsin at a ratio of 1:150 (w/w) (trypsin:protein) for 4 hours at 37°C, then digested overnight at room temperature using chymotrypsin at a ratio of 1:150 (w/w) (chymotrypsin:protein). Peptides were acidified to a final concentration of 1% TFA and desalted using C18 ZipTip (Millipore Sigma, ZTC185096). Dried peptides were resuspended in 10 µl of 0.1% TFA in water. Samples were then frozen and stored at -20°C until LC-MS analysis.

Liquid chromatography and mass spectrometry

A total of 250 ng of sample was injected (triplicate injections for cross-linked samples and duplicate injections for control samples) onto an UltiMate 3000 UHPLC system (Dionex, ThermoFisher Scientific). Peptides were trapped using an Acclaim PepMap C18 trapping column (ThermoFisher Scientific) using a load pump operating at 10 µL/min. Peptides were separated on a 200-cm µPAC C18 column (PharmaFluidics) using a linear gradient (1% solvent B for 4 min, 1 to 30% solvent B from 4 to 70 min, 30 to 55% solvent B from 70 to 90 min, 55 to 97% solvent B from 90 to 112 min, and isocratic at 97% solvent B from 112 to 120 min) at a flow rate of 800 nL/min. Gradient solvent A contained 0.1% formic acid, and solvent B contained 80% acetonitrile and 0.1% formic acid. LC eluate was interfaced to an Orbitrap Fusion Lumos Tribrid mass spectrometer (ThermoFisher Scientific) with a Nanospray Flex ion source (ThermoFisher Scientific). The source voltage was set to 2.5 kV, and the S-Lens RF level was set to 30%. Cross-links were identified using a previously described MS2-MS3 method[71] with slight modifications. Full scans were recorded from mass/charge ratio (m/z) 150 to 1500 at a resolution of 60,000 in the Orbitrap mass analyzer. The automatic gain control (AGC) target value was set to 4E5, and the maximum injection time was set to 50 ms in the Orbitrap. MS2 scans were recorded at a resolution of 30,000 in the Orbitrap mass analyzer. Only precursors with charge states between 4 and 8 were selected for MS2 scans. The AGC target was set to 5×10^4, a maximum injection time of 150 ms, and an isolation width of 1.6 m/z. Collision-induced dissociation fragmentation energy was set to 25%. The two most abundant reporter doublets from the MS2 scans with a charge state of 2 to 6, a 31.9721-Da mass difference, and a mass tolerance of ±10 parts per million (ppm) were selected for MS3. The MS3 scans were performed in the ion trap in rapid mode using higher-energy C-trap dissociation (HCD) fragmentation of 35% collision energy. The AGC target was set to 2×10^4, the maximum injection time was set to 200 ms, and the isolation width was set to 2.0 m/z.

Data analysis

To identify cross-linked peptides, Thermo *.raw files were imported into Proteome Discoverer 3.0 (ThermoFisher Scientific) and analyzed via XlinkX algorithm[72] using the MS2_MS3 workflow with the following parameters: MS1 mass tolerance, 10 ppm; MS2 mass tolerance, 20 ppm; MS3 mass tolerance, 0.5 Da; digestion: trypsin with four missed cleavages allowed; minimum peptide length: 4; variable modification: oxidation (M) and DSSO (K, S, T, and Y). The XlinkX/PD Validator node was used for cross-linked peptide validation with a 1% false discovery rate. Identified cross-links were further validated and quantified using Skyline (version 19.1)[73, 74] using a previously described protocol.[75] Cross-link spectral matches found in Proteome Discoverer were exported and converted to sequence spectrum list format using Excel (Microsoft). Cross-link peak areas were assessed using the MS1 full-scan filtering protocol for peaks within 8 min of the cross-link spectral match identification. Peak areas were assigned to the specified cross-linked peptide identification if the mass error was within 10 ppm of the theoretical mass, the isotope dot product was greater than 0.95, and the peak was not found in the non–cross-linked negative control samples. The isotope dot product compares the distribution of the measured MS1 signals against the theoretical isotope abundance distribution calculated based on the peptide sequence. Its value ranges between 0 and 1, where 1 indicates a perfect match.[76] Pairwise comparisons were made using the "MSstats" package (73) implemented in Skyline to calculate relative fold changes and significance. Significant change thresholds were defined as a log2 fold change less than −1 or greater than 1 and $-\log_{10}$ P value greater than 1.3 (P value less than 0.05). Visualization of proteins and cross-links was generated using xiNET.[77] Volcano plots were reformatted using Skyline output data within R with the tidyverse and ggplot2 packages.[78]

The data have been deposited to the ProteomeXchange Consortium via the PRIDE[70] partner repository with the dataset identifier PXDXXXXXX.

Structural Modeling.

PR models and combination PR:SRC3:p300 ternary models were generated using five independent runs with different seeds using the AlphaFold3.0 server.[53] The sequences provided were from the Uniprot P40601 isoforms for PR, Q9Y6Q9 for SRC3, and Q09472 for p300. The 32bp canonical PRE was modeled after the PRE used for crystallization experiments with the PR DBD[1] (RCSB:2C7A). Top models from each independent run were opened and aligned in ChimeraX (version 1.8[79-81]). Outputs were taken from HDXWorkbench[68] and overlayed onto the generated models. Models were selected based on HDXer[54] root mean square error (RMSE) values. HDXer was run using an automated server-based system to generate topology and gromacs files using the AMBER3.0 force fields. Topologies were then submitted to the server-based pipeline and RMSE values were generated from the differences between predicted and experimental deuterium exchange values.

Progesterone receptor response assays.

PR protein expression and response assays were co-transfected in 293T cells (ATCC, CRL-3216) at a 2:1 (protein:response plasmid) ratio using X-TremeGeneHP (Roche, XTGHP-RO) at a 4:1 (X-TremeGene:Plasmid Mix) ratio. Cells were incubated overnight, then re-seeded in 384-well plates in quadruplicate per transfected sample. Transfected cells were incubated for 4 hours at 37°C in a humidified 5% CO_2 incubator. After 4 hour incubation, either vehicle (EtOH), R5020 (Revvity, NLP004005MG), or RU486 (Sigma, M8046) at a final concentration of 50nM. Cells were incubated overnight with compound, then treated with dual-glo reagents (Promega), following a standard protocol. Plates were read on a Bio-Tek Neo II plate reader using a gain of 200 and integration time of 100ms.

Data Availability

Mass spectrometry data are available through the ProteomeXchange Consortium via the PRIDE partner repository under identifiers: PXDXXXXXX. Consolidated HDX-MS data are available through the hdxms.app web server. All other datasets generated and/ or analyzed during the current study are available from the corresponding author on reasonable request.

References

1. Roemer SC, Donham DC, Sherman L, Pon VH, Edwards DP, Churchill ME. Structure of the progesterone receptor-deoxyribonucleic acid complex: novel interactions required for binding to half-site response elements. Mol Endocrinol. 2006;20(12):3042-52. Epub 20060824. doi: 10.1210/me.2005-0511. PubMed PMID: 16931575; PMCID: PMC2532839.
2. Melvin VS, Harrell C, Adelman JS, Kraus WL, Churchill M, Edwards DP. The role of the C-terminal extension (CTE) of the estrogen receptor alpha and beta DNA binding domain in DNA binding and interaction with HMGB. J Biol Chem. 2004;279(15):14763-71. Epub 20040121. doi: 10.1074/jbc.M313335200. PubMed PMID: 14739282.
3. Hill KK, Roemer SC, Churchill MEA, Edwards DP. Structural and functional analysis of domains of the progesterone receptor. Molecular and Cellular Endocrinology. 2012;348(2):418-29. doi: 10.1016/j.mce.2011.07.017.
4. Grimm SL, Hartig SM, Edwards DP. Progesterone Receptor Signaling Mechanisms. J Mol Biol. 2016;428(19):3831-49. Epub 20160702. doi: 10.1016/j.jmb.2016.06.020. PubMed PMID: 27380738.
5. Simons SS, Edwards DP, Kumar R. Minireview: Dynamic Structures of Nuclear Hormone Receptors: New Promises and Challenges. Molecular Endocrinology. 2014;28(2):173-82. doi: 10.1210/me.2013-1334.
6. Mulac-Jericevic B, Lydon JP, Demayo FJ, Conneely OM. Defective mammary gland morphogenesis in mice lacking the progesterone receptor B isoform. Proceedings of the National Academy of Sciences. 2003;100(17):9744-9. doi: 10.1073/pnas.1732707100.
7. Fernandez-Valdivia R, Mukherjee A, Creighton CJ, Buser AC, DeMayo FJ, Edwards DP, Lydon JP. Transcriptional Response of the Murine Mammary Gland to Acute Progesterone Exposure. Endocrinology. 2008;149(12):6236-50. doi: 10.1210/en.2008-0768.
8. Aupperlee MD, Haslam SZ. Differential Hormonal Regulation and Function of Progesterone Receptor Isoforms in Normal Adult Mouse Mammary Gland. Endocrinology. 2007;148(5):2290-300. doi: 10.1210/en.2006-1721.
9. Zheng Z-H, Zhang G-L, Jiang R-F, Hong Y-Q, Zhang Q-Y, He J-P, Liu X-R, Yang Z-S, Yang L, Jiang X, Qu L-J, Ding C-H, Xu Y-W, Yang S-H, Liu J-L. METTL3 is essential for normal progesterone signaling during embryo implantation via m6A-mediated translation control of progesterone receptor. Proceedings of the National Academy of Sciences. 2023;120(5). doi: 10.1073/pnas.2214684120.
10. Takimoto GS, Tung L, Abdel-Hafiz H, Abel MG, Sartorius CA, Richer JK, Jacobsen BM, Bain DL, Horwitz KB. Functional properties of the N-terminal region of progesterone receptors and their mechanistic relationship to structure. J Steroid Biochem Mol Biol. 2003;85(2-5):209-19. doi: 10.1016/s0960-0760(03)00197-3. PubMed PMID: 12943706.
11. Lee SH, Yap YHY, Lim CL, Woo ARE, Lin VCL. Activation function 1 of progesterone receptor is required for mammary development and regulation of RANKL during pregnancy. Scientific Reports. 2022;12(1). doi: 10.1038/s41598-022-16289-x.
12. Vegeto E, Shahbaz MM, Wen DX, Goldman ME, O'Malley BW, McDonnell DP. Human progesterone receptor A form is a cell- and promoter-specific repressor of human progesterone receptor B function. Mol Endocrinol. 1993;7(10):1244-55. doi: 10.1210/mend.7.10.8264658. PubMed PMID: 8264658.
13. Lim CS, Baumann CT, Htun H, Xian W, Irie M, Smith CL, Hager GL. Differential Localization and Activity of the A- and B-Forms of the Human Progesterone Receptor Using Green Fluorescent Protein Chimeras. Molecular Endocrinology. 1999;13(3):366-75. doi: 10.1210/mend.13.3.0247.
14. Meyer ME, Quirin-Stricker C, Lerouge T, Bocquel MT, Gronemeyer H. A limiting factor mediates the differential activation of promoters by the human progesterone receptor isoforms. Journal of Biological Chemistry. 1992;267(15):10882-7. doi: 10.1016/s0021-9258(19)50100-4.
15. Takimoto GS, Hovland AR, Tasset DM, Melville MY, Tung L, Horwitz KB. Role of Phosphorylation on DNA Binding and Transcriptional Functions of Human Progesterone Receptors. Journal of Biological Chemistry. 1996;271(23):13308-16. doi: 10.1074/jbc.271.23.13308.
16. Truong TH, Dwyer AR, Diep CH, Hu H, Hagen KM, Lange CA. Phosphorylated Progesterone Receptor Isoforms Mediate Opposing Stem Cell and Proliferative Breast Cancer Cell Fates. Endocrinology. 2019;160(2):430-46. doi: 10.1210/en.2018-00990. PubMed PMID: 30597041; PMCID: PMC6349004.

17. Cartwright M, Louw-du Toit R, Jackson H, Janse van Vuuren M, Africander D. Progesterone receptor isoform ratios influence the transcriptional activity of progestins via the progesterone receptor. J Steroid Biochem Mol Biol. 2023;232:106348. Epub 20230612. doi: 10.1016/j.jsbmb.2023.106348. PubMed PMID: 37315868.
18. Wargon V, Riggio M, Giulianelli S, Sequeira GR, Rojas P, May M, Polo ML, Gorostiaga MA, Jacobsen B, Molinolo A, Novaro V, Lanari C. Progestin and antiprogestin responsiveness in breast cancer is driven by the PRA/PRB ratioviaAIB1 or SMRT recruitment to theCCND1andMYCpromoters. International Journal of Cancer. 2015;136(11):2680-92. doi: 10.1002/ijc.29304.
19. Graham JD, Yeates C, Balleine RL, Harvey SS, Milliken JS, Bilous AM, Clarke CL. Characterization of Progesterone Receptor A and B Expression in Human Breast Cancer1. Cancer Research. 1995;55(21):5063-8.
20. Graham JD, Yager ML, Hill HD, Byth K, O'Neill GM, Clarke CL. Altered Progesterone Receptor Isoform Expression Remodels Progestin Responsiveness of Breast Cancer Cells. Molecular Endocrinology. 2005;19(11):2713-35. doi: 10.1210/me.2005-0126.
21. Joshi PA, Jackson HW, Beristain AG, Di Grappa MA, Mote PA, Clarke CL, Stingl J, Waterhouse PD, Khokha R. Progesterone induces adult mammary stem cell expansion. Nature. 2010;465(7299):803-7. doi: 10.1038/nature09091.
22. Asselin-Labat M-L, Vaillant F, Sheridan JM, Pal B, Wu D, Simpson ER, Yasuda H, Smyth GK, Martin TJ, Lindeman GJ, Visvader JE. Control of mammary stem cell function by steroid hormone signalling. Nature. 2010;465(7299):798-802. doi: 10.1038/nature09027.
23. Axlund SD, Sartorius CA. Progesterone regulation of stem and progenitor cells in normal and malignant breast. Molecular and Cellular Endocrinology. 2012;357(1-2):71-9. doi: 10.1016/j.mce.2011.09.021.
24. Pathiraja TN, Shetty PB, Jelinek J, He R, Hartmaier R, Margossian AL, Hilsenbeck SG, Issa J-PJ, Oesterreich S. Progesterone Receptor Isoform-Specific Promoter Methylation: Association of PRA Promoter Methylation with Worse Outcome in Breast Cancer Patients. Clinical Cancer Research. 2011;17(12):4177-86. doi: 10.1158/1078-0432.ccr-10-2950.
25. Huggins C, Moon RC, Morii S. EXTINCTION OF EXPERIMENTAL MAMMARY CANCER, I. ESTRADIOL-17β AND PROGESTERONE. Proceedings of the National Academy of Sciences. 1962;48(3):379-86. doi: 10.1073/pnas.48.3.379.
26. Collaborative Group on Hormonal Factors in Breast C. Type and timing of menopausal hormone therapy and breast cancer risk: individual participant meta-analysis of the worldwide epidemiological evidence. Lancet. 2019;394(10204):1159-68. Epub 20190829. doi: 10.1016/S0140-6736(19)31709-X. PubMed PMID: 31474332; PMCID: PMC6891893.
27. Williams SP, Sigler PB. Atomic structure of progesterone complexed with its receptor. Nature. 1998;393(6683):392-6. doi: 10.1038/30775.
28. Raaijmakers HCA, Versteegh JE, Uitdehaag JCM. The X-ray Structure of RU486 Bound to the Progesterone Receptor in a Destabilized Agonistic Conformation. Journal of Biological Chemistry. 2009;284(29):19572-9. doi: 10.1074/jbc.m109.007872.
29. Petit-Topin I, Fay M, Resche-Rigon M, Ulmann A, Gainer E, Rafestin-Oblin ME, Fagart J. Molecular determinants of the recognition of ulipristal acetate by oxo-steroid receptors. J Steroid Biochem Mol Biol. 2014;144 Pt B:427-35. Epub 20140906. doi: 10.1016/j.jsbmb.2014.08.008. PubMed PMID: 25204619.
30. Edwards DP, Kühnel B, Estes PA, Nordeen SK. Human Progesterone Receptor Binding to Mouse Mammary Tumor Virus Deoxyribonucleic Acid: Dependence on Hormone and Nonreceptor Nuclear Factor(s). Molecular Endocrinology. 1989;3(2):381-91. doi: 10.1210/mend-3-2-381.
31. Klein-Hitpass L, Tsai SY, Weigel NL, Allan GF, Riley D, Rodriguez R, Schrader WT, Tsai MJ, O'Malley BW. The progesterone receptor stimulates cell-free transcription by enhancing the formation of a stable preinitiation complex. Cell. 1990;60(2):247-57. doi: 10.1016/0092-8674(90)90740-6. PubMed PMID: 2153462.
32. Lieberman BA, Bona BJ, Edwards DP, Nordeen SK. The constitution of a progesterone response element. Molecular Endocrinology. 1993;7(4):515-27. doi: 10.1210/mend.7.4.8388996.
33. Zhang Z, Smith DL. Determination of amide hydrogen exchange by mass spectrometry: A new tool for protein structure elucidation. Protein Science. 1993;2(4):522-31. doi: 10.1002/pro.5560020404.
34. Bai Y, Milne JS, Mayne L, Englander SW. Primary structure effects on peptide group hydrogen exchange. Proteins: Structure, Function, and Genetics. 1993;17(1):75-86. doi: 10.1002/prot.340170110.
35. Chalmers MJ, Busby SA, Pascal BD, He Y, Hendrickson CL, Marshall AG, Griffin PR. Probing protein ligand interactions by automated hydrogen/deuterium exchange mass spectrometry. Anal Chem. 2006;78(4):1005-14. doi: 10.1021/ac051294f. PubMed PMID: 16478090.

36. Wales TE, Engen JR. Hydrogen exchange mass spectrometry for the analysis of protein dynamics. Mass Spectrometry Reviews. 2006;25(1):158-70. doi: 10.1002/mas.20064.
37. Zheng J, Strutzenberg T, Pascal BD, Griffin PR. Protein dynamics and conformational changes explored by hydrogen/deuterium exchange mass spectrometry. Current Opinion in Structural Biology. 2019;58:305-13. doi: 10.1016/j.sbi.2019.06.007.
38. Hofmann T, Fischer AW, Meiler J, Kalkhof S. Protein structure prediction guided by crosslinking restraints – A systematic evaluation of the impact of the crosslinking spacer length. Methods. 2015;89:79-90. doi: 10.1016/j.ymeth.2015.05.014.
39. Chavez JD, Lee CF, Caudal A, Keller A, Tian R, Bruce JE. Chemical Crosslinking Mass Spectrometry Analysis of Protein Conformations and Supercomplexes in Heart Tissue. Cell Systems. 2018;6(1):136-41.e5. doi: 10.1016/j.cels.2017.10.017.
40. Schneider M, Belsom A, Rappsilber J. Protein Tertiary Structure by Crosslinking/Mass Spectrometry. Trends in Biochemical Sciences. 2018;43(3):157-69. doi: 10.1016/j.tibs.2017.12.006.
41. Brodie NI, Sarpe V, Crowder DA, Schriemer D. All-in-One Pseudo-MS³ Method for the Analysis of Gas-Phase Cleavable Protein Crosslinking Reactions. Journal of the American Society for Mass Spectrometry. 2023;34(10):2146-55. doi: 10.1021/jasms.3c00134.
42. Elliston JF, Beekman JM, Tsai SY, O'Malley BW, Tsai MJ. Hormone activation of baculovirus expressed progesterone receptors. Journal of Biological Chemistry. 1992;267(8):5193-8. doi: 10.1016/s0021-9258(18)42750-0.
43. Beck CA, Zhang Y, Altmann M, Weigel NL, Edwards DP. Stoichiometry and site-specific phosphorylation of human progesterone receptor in native target cells and in the baculovirus expression system. J Biol Chem. 1996;271(32):19546-55. doi: 10.1074/jbc.271.32.19546. PubMed PMID: 8702648.
44. Christensen K, Estes PA, Onate SA, Beck CA, DeMarzo A, Altmann M, Lieberman BA, St John J, Nordeen SK, Edwards DP. Characterization and functional properties of the A and B forms of human progesterone receptors synthesized in a baculovirus system. Mol Endocrinol. 1991;5(11):1755-70. doi: 10.1210/mend-5-11-1755. PubMed PMID: 1779977.
45. Wardell SE, Kwok SC, Sherman L, Hodges RS, Edwards DP. Regulation of the Amino-Terminal Transcription Activation Domain of Progesterone Receptor by a Cofactor-Induced Protein Folding Mechanism. Molecular and Cellular Biology. 2005;25(20):8792-808. doi: 10.1128/mcb.25.20.8792-8808.2005.
46. Kumar R, Moure CM, Khan SH, Callaway C, Grimm SL, Goswami D, Griffin PR, Edwards DP. Regulation of the Structurally Dynamic N-terminal Domain of Progesterone Receptor by Protein-induced Folding. Journal of Biological Chemistry. 2013;288(42):30285-99. doi: 10.1074/jbc.m113.491787.
47. Goswami D, Callaway C, Pascal D, Bruce, Kumar R, Edwards P, Dean, Griffin R, Patrick. Influence of Domain Interactions on Conformational Mobility of the Progesterone Receptor Detected by Hydrogen/Deuterium Exchange Mass Spectrometry. Structure. 2014;22(7):961-73. doi: 10.1016/j.str.2014.04.013.
48. Rayasam GV, Elbi C, Walker DA, Wolford R, Fletcher TM, Edwards DP, Hager GL. Ligand-Specific Dynamics of the Progesterone Receptor in Living Cells and during Chromatin Remodeling In Vitro. Molecular and Cellular Biology. 2005;25(6):2406-18. doi: 10.1128/mcb.25.6.2406-2418.2005.
49. Zhang Y, Beck CA, Poletti A, Clement JP, IV, Prendergast P, Yip T-T, Hutchens TW, Edwards DP, Weigel NL. Phosphorylation of Human Progesterone Receptor by Cyclin-Dependent Kinase 2 on Three Sites That Are Authentic Basal Phosphorylation Sites In Vivo. Molecular Endocrinology. 1997;11(6):823-32. doi: 10.1210/mend.11.6.0006.
50. Schmidt TG, Skerra A. The Strep-tag system for one-step purification and high-affinity detection or capturing of proteins. Nature Protocols. 2007;2(6):1528-35. doi: 10.1038/nprot.2007.209.
51. Yu X, Yi P, Panigrahi AK, Lumahan LEV, Lydon JP, Lonard DM, Ludtke SJ, Wang Z, O'Malley BW. Spatial definition of the human progesterone receptor-B transcriptional complex. iScience. 2022;25(11):105321. doi: 10.1016/j.isci.2022.105321.
52. Abramson J, Adler J, Dunger J, Evans R, Green T, Pritzel A, Ronneberger O, Willmore L, Ballard AJ, Bambrick J, Bodenstein SW, Evans DA, Hung CC, O'Neill M, Reiman D, Tunyasuvunakool K, Wu Z, Zemgulyte A, Arvaniti E, ..., Jumper JM. Accurate structure prediction of biomolecular interactions with AlphaFold 3. Nature. 2024. Epub 20240508. doi: 10.1038/s41586-024-07487-w. PubMed PMID: 38718835.
53. Abramson J, Adler J, Dunger J, Evans R, Green T, Pritzel A, Ronneberger O, Willmore L, Ballard AJ, Bambrick J, Bodenstein SW, Evans DA, Hung C-C, O'Neill M, Reiman D, Tunyasuvunakool K, Wu Z, Žemgulytė

A, Arvaniti E, ..., Jumper JM. Accurate structure prediction of biomolecular interactions with AlphaFold 3. Nature. 2024. doi: 10.1038/s41586-024-07487-w.
54. Lee PS, Bradshaw RT, Marinelli F, Kihn K, Smith A, Wintrode PL, Deredge DJ, Faraldo-Gomez JD, Forrest LR. Interpreting Hydrogen-Deuterium Exchange Experiments with Molecular Simulations: Tutorials and Applications of the HDXer Ensemble Reweighting Software [Article v1.0]. Living J Comput Mol Sci. 2021;3(1). Epub 20220126. doi: 10.33011/livecoms.3.1.1521. PubMed PMID: 36644498; PMCID: PMC9835200.
55. Heery DM, Hoare S, Hussain S, Parker MG, Sheppard H. Core LXXLL Motif Sequences in CREB-binding Protein, SRC1, and RIP140 Define Affinity and Selectivity for Steroid and Retinoid Receptors. Journal of Biological Chemistry. 2001;276(9):6695-702. doi: 10.1074/jbc.m009404200.
56. Kattoula SR, Baker ME. Structural and evolutionary analysis of the co-activator binding domain in vertebrate progesterone receptors. J Steroid Biochem Mol Biol. 2014;141:7-15. Epub 20131231. doi: 10.1016/j.jsbmb.2013.12.018. PubMed PMID: 24388949.
57. Ding XF, Anderson CM, Ma H, Hong H, Uht RM, Kushner PJ, Stallcup MR. Nuclear receptor-binding sites of coactivators glucocorticoid receptor interacting protein 1 (GRIP1) and steroid receptor coactivator 1 (SRC-1): multiple motifs with different binding specificities. Mol Endocrinol. 1998;12(2):302-13. doi: 10.1210/mend.12.2.0065. PubMed PMID: 9482670.
58. Aarts MT, Wagner M, Van Der Wal T, Van Boxtel AL, Van Amerongen R. A molecular toolbox to study progesterone receptor signaling. Journal of Mammary Gland Biology and Neoplasia. 2023;28(1). doi: 10.1007/s10911-023-09550-0.
59. Edwards DP, Altmann M, DeMarzo A, Zhang Y, Weigel NL, Beck CA. Progesterone receptor and the mechanism of action of progesterone antagonists. J Steroid Biochem Mol Biol. 1995;53(1-6):449-58. doi: 10.1016/0960-0760(95)00091-d. PubMed PMID: 7626494.
60. Leonhardt SA, Altmann M, Edwards DP. Agonist and Antagonists Induce Homodimerization and Mixed Ligand Heterodimerization of Human Progesterone Receptors in Vivo by a Mammalian Two-Hybrid Assay. Molecular Endocrinology. 1998;12(12):1914-30. doi: 10.1210/mend.12.12.0210.
61. Allan GF, Leng X, Tsai SY, Weigel NL, Edwards DP, Tsai MJ, O'Malley BW. Hormone and antihormone induce distinct conformational changes which are central to steroid receptor activation. Journal of Biological Chemistry. 1992;267(27):19513-20. doi: 10.1016/s0021-9258(18)41805-4.
62. Weigel NL, Beck CA, Estes PA, Prendergast P, Altmann M, Christensen K, Edwards DP. Ligands induce conformational changes in the carboxyl-terminus of progesterone receptors which are detected by a site-directed antipeptide monoclonal antibody. Molecular Endocrinology. 1992;6(10):1585-97. doi: 10.1210/mend.6.10.1448113.
63. Madauss KP, Grygielko ET, Deng SJ, Sulpizio AC, Stanley TB, Wu C, Short SA, Thompson SK, Stewart EL, Laping NJ, Williams SP, Bray JD. A structural and in vitro characterization of asoprisnil: a selective progesterone receptor modulator. Mol Endocrinol. 2007;21(5):1066-81. Epub 20070313. doi: 10.1210/me.2006-0524. PubMed PMID: 17356170.
64. Meyer ME, Pornon A, Ji JW, Bocquel MT, Chambon P, Gronemeyer H. Agonistic and antagonistic activities of RU486 on the functions of the human progesterone receptor. EMBO J. 1990;9(12):3923-32. doi: 10.1002/j.1460-2075.1990.tb07613.x. PubMed PMID: 2249658; PMCID: PMC552163.
65. Vegeto E, Allan GF, Schrader WT, Tsai MJ, McDonnell DP, O'Malley BW. The mechanism of RU486 antagonism is dependent on the conformation of the carboxy-terminal tail of the human progesterone receptor. Cell. 1992;69(4):703-13. doi: 10.1016/0092-8674(92)90234-4. PubMed PMID: 1586949.
66. Wang D, Simons SS, Jr. Corepressor binding to progesterone and glucocorticoid receptors involves the activation function-1 domain and is inhibited by molybdate. Mol Endocrinol. 2005;19(6):1483-500. Epub 20050317. doi: 10.1210/me.2005-0012. PubMed PMID: 15774497.
67. Xu J, Nawaz Z, Tsai SY, Tsai MJ, O'Malley BW. The extreme C terminus of progesterone receptor contains a transcriptional repressor domain that functions through a putative corepressor. Proceedings of the National Academy of Sciences. 1996;93(22):12195-9. doi: 10.1073/pnas.93.22.12195.
68. Pascal BD, Willis S, Lauer JL, Landgraf RR, West GM, Marciano D, Novick S, Goswami D, Chalmers MJ, Griffin PR. HDX Workbench: Software for the Analysis of H/D Exchange MS Data. Journal of the American Society for Mass Spectrometry. 2012;23(9):1512-21. doi: 10.1007/s13361-012-0419-6.
69. Keppel TR, Weis DD. Mapping Residual Structure in Intrinsically Disordered Proteins at Residue Resolution Using Millisecond Hydrogen/Deuterium Exchange and Residue Averaging. Journal of the American Society for Mass Spectrometry. 2015;26(4):547-54. doi: 10.1007/s13361-014-1033-6.

70. Perez-Riverol Y, Csordas A, Bai J, Bernal-Llinares M, Hewapathirana S, Kundu DJ, Inuganti A, Griss J, Mayer G, Eisenacher M, Perez E, Uszkoreit J, Pfeuffer J, Sachsenberg T, Yilmaz S, Tiwary S, Cox J, Audain E, Walzer M, ..., Vizcaino JA. The PRIDE database and related tools and resources in 2019: improving support for quantification data. Nucleic Acids Res. 2019;47(D1):D442-D50. doi: 10.1093/nar/gky1106. PubMed PMID: 30395289; PMCID: PMC6323896.
71. Liu F, Lössl P, Scheltema R, Viner R, Heck AJR. Optimized fragmentation schemes and data analysis strategies for proteome-wide cross-link identification. Nature Communications. 2017;8(1):15473. doi: 10.1038/ncomms15473.
72. Liu F, Rijkers DTS, Post H, Heck AJR. Proteome-wide profiling of protein assemblies by cross-linking mass spectrometry. Nature Methods. 2015;12(12):1179-84. doi: 10.1038/nmeth.3603.
73. Pino LK, Searle BC, Bollinger JG, Nunn B, MacLean B, MacCoss MJ. The Skyline ecosystem: Informatics for quantitative mass spectrometry proteomics. Mass Spectrometry Reviews. 2020;39(3):229-44. doi: https://doi.org/10.1002/mas.21540.
74. MacLean B, Tomazela DM, Shulman N, Chambers M, Finney GL, Frewen B, Kern R, Tabb DL, Liebler DC, MacCoss MJ. Skyline: an open source document editor for creating and analyzing targeted proteomics experiments. Bioinformatics. 2010;26(7):966-8. Epub 20100209. doi: 10.1093/bioinformatics/btq054. PubMed PMID: 20147306; PMCID: PMC2844992.
75. Chen Z, Chen Z, Rappsilber J. A generic solution for quantifying cross-linked peptides using software Skyline. Protocol Exchange. 2018. doi: 10.1038/protex.2018.001.
76. Chen ZA, Rappsilber J. Quantitative cross-linking/mass spectrometry to elucidate structural changes in proteins and their complexes. Nature Protocols. 2019;14(1):171-201. doi: 10.1038/s41596-018-0089-3.
77. Combe CW, Fischer L, Rappsilber J. xiNET: Cross-link Network Maps With Residue Resolution. Molecular & Cellular Proteomics. 2015;14(4):1137-47. doi: 10.1074/mcp.o114.042259.
78. Wickham H, Averick M, Bryan J, Chang W, McGowan L, François R, Grolemund G, Hayes A, Henry L, Hester J, Kuhn M, Pedersen T, Miller E, Bache S, Müller K, Ooms J, Robinson D, Seidel D, Spinu V, ..., Yutani H. Welcome to the Tidyverse. Journal of Open Source Software. 2019;4(43). doi: 10.21105/joss.01686.
79. Goddard TD, Huang CC, Meng EC, Pettersen EF, Couch GS, Morris JH, Ferrin TE. UCSF ChimeraX: Meeting modern challenges in visualization and analysis. Protein Science. 2018;27(1):14-25. doi: 10.1002/pro.3235.
80. Pettersen EF, Goddard TD, Huang CC, Meng EC, Couch GS, Croll TI, Morris JH, Ferrin TE. <scp>UCSF ChimeraX</scp>: Structure visualization for researchers, educators, and developers. Protein Science. 2021;30(1):70-82. doi: 10.1002/pro.3943.
81. Meng EC, Goddard TD, Pettersen EF, Couch GS, Pearson ZJ, Morris JH, Ferrin TE. <scp>UCSF ChimeraX</scp>: Tools for structure building and analysis. Protein Science. 2023;32(11). doi: 10.1002/pro.4792.